UNIVERSITÀ DEGLI STUDI DI PADOVA

DIPARTIMENTO DI INGEGNERIA INDUSTRIALE

CORSO DI LAUREA MAGISTRALE IN INGEGNERIA DEI MATERIALI

Tesi di Laurea Magistrale in

Ingegneria dei Materiali

REDUCTION BEHAVIOR OF CHROMIUM AND TITANIUM ALLOYED CARBON FREE POWDER STEELS

Relatore: Prof. Giorgio Pavesi

Correlatore: Prof. Manuele Dabalà

Laureando: Mirko Pinarello

ANNO ACCADEMICO 2014/2015

RUHR-UNIVERSITÄT BOCHUM

RUB

Reduction Behavior of Chromium and Titanium Alloyed Carbon free Powder Steels

Masterarbeit

vorgelegt dem
Lehrstuhl Werkstofftechnik
(Prof. Dr.-Ing. W. Theisen)

der
Fakultät für Maschinenbau
der Ruhr–Universität Bochum

von
Mirko Pinarello

Bochum 2014

Gutachter:	Prof. Dr.-Ing. W. Theisen
	Prof. Dr.-Ing. S. Huth
Betreuerin:	M.Sc. A. Weddeling

Abstract

The constant increase of requirements for PM-parts leads to a major complexity of the chemical composition of powders, by alloying several elements into powder steels, and an improvement of mechanical properties by fine dispersion of carbides as hard phase. The presence in alloys of elements with high oxygen affinity like Chromium, Vanadium and Iron itself, and the high specific surface of powders exposed to air cause the formation of thermodynamically stable oxide phases on the powders surface. An oxide layer on powder surfaces is regularly unwanted since it acts as diffusion barrier during the sintering process, reducing inter-particle cohesion and the final mechanical properties of the sintered parts. Thermodynamic considerations indicate carbon monoxide developed by the direct carbothermal reduction as the most effective reducing agent due to the constant decrease of the Gibbs free-energy with the increase of the temperature. Thus it would be reasonable concluding that the complete reduction of oxides can be achieved with the addition of higher percentages of carbon in form of graphite.

This work deals with the investigation and the comprehension of the reduction behavior of oxide phase in chromium and titanium alloyed carbon-free powder steels heated under vacuum conditions with different amounts of carbon admixed before sintering.

Data acquired by RGA experiments indicate an evident connection between carbon admixed and gaseous evolution from carbothermal reduction of metal oxides. Analysis on the powder surface with SEM and EDX shows that the effect of graphite addition depends on the type of the powder, suggesting that higher carbon content does not systematically lead to improved sintering properties.

Contents

Chapter 1

Introduction

Powder metallurgy is a metallurgical production technique that has assumed remarkable importance during the last two centuries especially for the fabrication of materials that cannot be produced by conventional technology. Examples of these materials are mechanical components and work tools steels with complex shape, specific properties or refractory metals phases (W, Mo, Ti, Nb, V due to the high thermodynamically stability of their compounds). In these cases, the preparation by powder metallurgy procedures is technically and economically favorable. A wide range of interesting fields and the great flexibility of the manufacturing process, determined the rapid rise of powder metallurgy industry.

The constant increase of requirements for PM-parts leads to a major complexity of the chemical composition of powders, by alloying several elements into powder steels, and an improvement of mechanical properties by fine dispersion of hard phases and prevention of major segregations. In the case of tools steels the main property required is corrosion and wear resistance. Corrosion resistance is obtained by alloying a relevant amount of Chromium in alloy (12% mass). Wear resistance can be provided by the fine dispersion of carbides as hard phase. The presence in alloys of elements with high oxygen affinity like Chromium, Vanadium and Iron itself, and the high specific surface of powders exposed to air cause the formation of thermodynamically stable oxide phases on the powders surface. An oxide layer on powder surfaces is regularly unwanted since it acts as diffusion barrier during the sintering process, reducing inter-particle cohesion and the final mechanical properties of the sintered parts. The stability of carbides (especially Titanium or Niobium carbides) makes the atomization of pre-alloyed melt impossible due to primarily precipitation of carbides with uncontrolled size, determining the risk of nozzle clogging in the atomization unit. New methods have been developed and the In-Situ carbide formation in carbon-free powder steels by diffusion alloying is currently under investigation.

Diffusion plays a key role in both processes of sintering and carbon-uptake for the formation of carbides; the reduction of metal oxide layers on the powder surface must be achieved priorly but the mechanism and the complete control of the process are still not well reached. The reduction of the metal oxides takes place by heating the powder in reducing agents atmosphere. The most common technologies involve hydrogen and carbon as reducing agents and in particular way the carbothermal reduction is the most effective for high alloyed powder steels. During the reduction process, a gas phase is obviously developed and the analysis of the gas evolution by residual gas analyzer offers one approach to study the process of sintering. This thesis deals with the investigation and the comprehension of the reduction behavior of oxide phase in Chromium and Titanium alloyed carbon-free powder steels heated under vacuum conditions with different amounts of carbon admixed before sintering.
The thesis is organized as follows:

- The second chapter, after the introduction, concerns on providing theoretical backgrounds necessary for a general understanding of topic.
- In the third chapter aims and way of the research are reported whereas the fourth chapter presents the materials used and the methodology decided for the investigation.
- Chapters numbers 5 and 6 feature the results obtained and the discussion of them taking into account previous studies and researches.
- The last chapter regards the summary of the thesis and possible perspectives.

Chapter 2

Backgrounds

2.1 Powder Metallurgy

Research and development in powder metallurgy (PM) materials are constantly focused on fulfilling quality, cost and performance requirements of existing and innovative applications. PM technology is based on a densification process of the steel powder normally through a pressing operation producing a 'green' compact and a subsequent heat treatment (sintering) below the liquidus temperature so that the powder particles can bond together. The minimal dimensional change of the compact after sintering and the characteristics of a near net-shape technology make the PM process very competitive for the production of structural steels parts. Furthermore, other key attributes as minimal loss of material, low energy consumption and short production time determinate that the manufacturing cost is usually lower when compared to other technologies.

The conventional PM process diagram is shown in Fig. 2.1. Starting from the production of powder, the main process stages are mixing, compaction and sintering, which are shortly described below. After the sintering process, there are supplementary operations which may be conducted in order to increase density by eliminating microporosity, improve dimensional tolerance, enhance strength (i.e. by infiltration of liquid metal with lower melting point) and donate further wear resistance layer deposed on the surface.

There are several ways to produce PM components and manufacturing innovations regard nowadays all steps of the process, including new alloying systems, more efficient compaction techniques and rising the limit of the maximum sintering temperature.

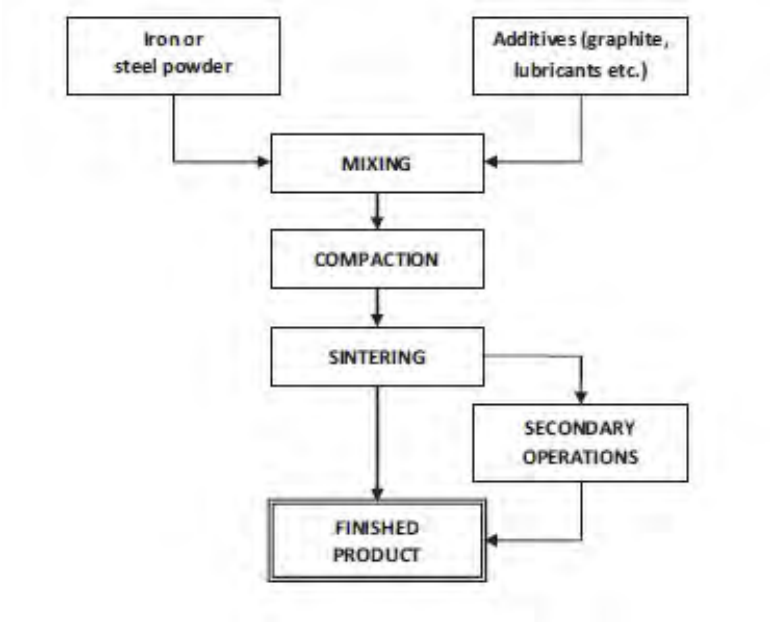

Figure 2.1: Operating Diagram of Powder Metallurgy [14]

2.1.1 Production of powder

The fundamental factor behind the powder production is the necessary energy that must be delivered to the material for the creation of new surface area. There are many ways to produce metal powder:

- Comminution of solid metal, which consists on a mechanical size reduction of the materials by the actions of milling rolls without a phase change;
- Thermal decomposition of a gaseous chemical compound formed by reaction of metal with gas under pressure, obtaining very fine powder (i.e. Carbonyl Process) or the chemical precipitation of metal from a solution of a soluble salt;
- Reduction of a compound, usually an oxide, in solid state. In this typical production of iron powder, the selected ore is crushed, mixed with carbon, and passed through a continuous furnace where reaction takes place leaving agglomerates of sponge iron which are then further treated by crushing, separation of non-metallic material, and sieving to produce powder;
- Electrodeposition of metals in spongy or powdery state in a solution under suitable conditions of density, temperature, current density and composition of the electrolyte. The process involves further operations such washing, drying and usually crushing;

- and the Atomization of molten metal.[15]

The last process listed is the most used in the case of stainless or high alloyed steel powders. Since the powders utilized are produced through this technique, a more detailed description follows in the next paragraph.

Atomization process

The principal method is to disintegrate a thin stream of molten metal by the impact of a high pressure liquid or gas jet. Air, nitrogen and argon are commonly used gases, whereas water is the liquid most widely used. The molten metal stream is forced through an orifice (nozzle) at moderate pressures. The jet is introduced when the melt is leaving the nuzzle, creating a turbulence related to the rapid expansion of the fluid caused by the temperature difference, disintegrating the molten flow. The resulting droplets are rapidly solidified for avoiding welds from the contact of the particles and their agglomeration. The large collection volume is usually filled with gas promoting further turbulence (Fig. 2. 2).

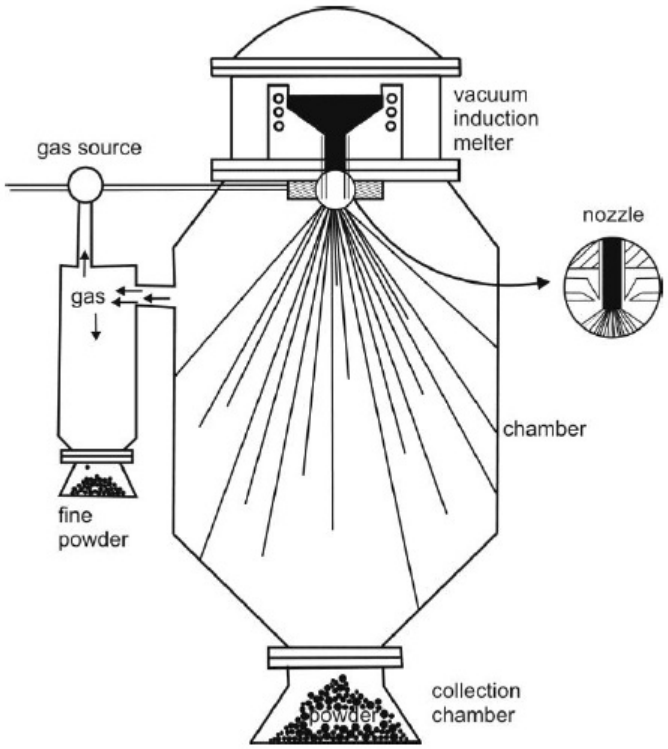

Figure 2. 2: Manufacturing scheme of a gas atomization [16]

By varying several parameters as design and configuration of the nozzle, pressure and volume

of the atomizing fluid, thickness of the stream of molten metal, it is furthermore possible to control the particle size distribution over a wide range. The particles shape depends mostly on the solidification of the molten metal droplets and the nature of the fluid used. In the case of a melt atomized with a liquid (water), the powder surfaces appear very irregular and rough, whereas the gas atomized powder presents a regular spherical shape. Although the higher specific surface and the irregular shape promotes the compressibility and sintering ability, on the other hand water is a very aggressive oxidation agent, causing the formation of a thick and stable oxide layer on the surfaces which deteriorates the cohesion of particles and the mechanical properties of the component. Water atomization is widely used for the production of iron or low alloyed powder steel and gas atomization has been established as the preferable method for high alloyed steels and superalloys.

2.1.2 Mixing and compaction process

The intention of the mixing process is to have a homogeneous mixture of metal powder and lubricant. Lubricant is added in order to reduce the friction between the particles and the walls of the die, reducing the possibility to have differences on density in the compacted part and enhance the ejection of the compact itself, preventing the formation of cracks. In fact, it has already been proved that the friction of the particles with the walls decreases exponentially the pressure transmitted to the powders along the compacting direction, making an effort to the development and the innovation of the pressing design. However, despite the evident benefits provided by the presence of the lubricant, it leads also to a limit of the achievable density, which usually can not exceed 95% for mostly all types of powder.
New variants of the compaction step have been developed, i.e. warm compaction, isostatic pressing or high velocity compaction. In the warm compaction, both powder and compaction tooling are pre-heated to 130 °C , obtaining an increase of the green density and sensibly the mechanical properties after sintering by 10-20% [15].

Cold and Hot Isostatic Pressing

With respect to conventional forming techniques, in isostatic pressing (IP) the powder is confined within a flexible membrane or a hermetic container and subjecting to the pressure of

a surrounding medium, liquid or gas. The usage of a pressurizing fluid guarantees an uniform compacting action on the powder, avoiding furthermore the direct contact with the die. In Cold IP the process occurs at room temperature, the membrane is usually a plastic material and the fluid utilized is water or oil. The compacted part still requires a sintering process.
For Hot Isostatic Pressing (HIP), the container is made of metal or glass and the medium is an inert gas as argon or helium. At the elevated temperatures of the process, the container deforms plastically compacting the powder. The combination of heat and pressure eliminates the need for a supplemental sintering step.
This method is suitable for large size parts, with no virtual limit on geometric complexity. Furthermore, it currently is the preferable way to compact expensive materials such as superalloys, titanium, tool steels, stainless steel which find many applications in military, aerospace and automotive environments [17].

2.1.3 Sintering

In this process the elevated temperatures allow the particles to bond together through mass transfer mechanisms. The compact acquires the strength and the properties needed to fulfill the requirements for engineering and structural applications.
Other phenomena as recrystallization and grain growth may follow and the pores tend to become round and isolated, with a general decrease of the total porosity of the compact. In this stage, plastic deformation occurs as well, contributing to the atoms mobility.

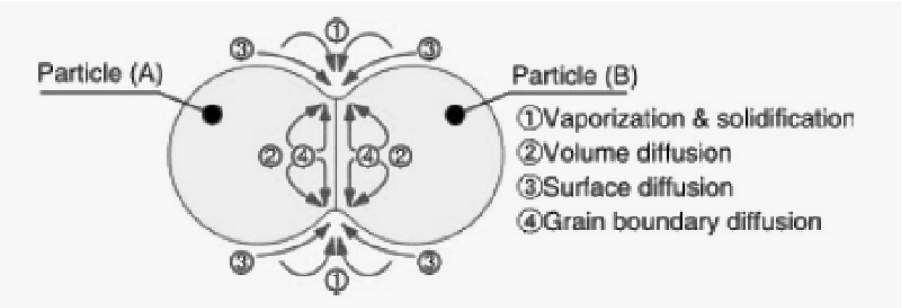

Figure 2. 3: Mass transfer mechanisms during sintering

The mechanisms are reported in Fig.2. 3 and the most relevant is diffusion.

Diffusion

In a mixture, diffusion always occurs in order to decrease the difference in concentration of species, according to a certain chemical potential gradient. According to a general manner, this is accomplished with material transport of atoms from a region of higher potential to a region of lower potential, obtaining a decrease of Gibbs free-energy of the system.
In a lattice of a metal matrix the most important diffusion mechanisms are interstitial diffusion and vacancy diffusion. Interstitial diffusion involves jumping of atoms from an interstitial position to an adjacent position. In vacancy diffusion (substitutional diffusion) an atom from normal lattice position jumps into adjacent vacant position, with a consequent opposite flow of the vacancy itself. Interstitial diffusion is much faster than vacancy diffusion.
The net flow of atoms decreasing the concentration gradient when a steady state exist, that is when concentration of every point does not change with time, is given by Ficks first law as

$$J = -D\frac{\delta C}{\delta x} \tag{2.1}$$

Where J is the net flow or diffusive flux, D is known as diffusion coefficient and $\frac{\delta C}{\delta x}$ is the concentration gradient.
For non-steady state change in concentration with time can be predicted using Ficks second law:

$$\frac{\delta C}{\delta t} = D\frac{\delta^2 C}{\delta x^2} \tag{2.2}$$

The diffusion coefficient D is independent of composition and it depends exponentially on Temperature following Arrhenius law.

$$D = D_0 exp(-\frac{Q}{RT}); \tag{2.3}$$

T is the temperature expressed in K, R is the universal gas constant, Do is a constant characteristic of the material and Q is the activation energy necessary for the process.

Differently from the powders production process, in which the energy is provided from external source to increase the total surface, the driving force of the thermally activated sintering process is the surface energy difference between the initial and final state.
Among the mechanisms shown in Fig. 2.3, the transfer via evaporation-deposition is not relevant

for most metals because of the lower values of vapor pressure near the melting point of the metals. The basic principle is that the equilibrium vapor pressure over a concave surface is lower compared to that of a convex surface, resulting on a mass flow along the vapor pressure gradient [18]. As can be seen in the Fig.2. 4 beside, which presents the different velocities of the diffusion mechanisms, the fastest transport of atoms occurs via surface, evidencing therefore the importance of the reduction of the oxides layer on it.

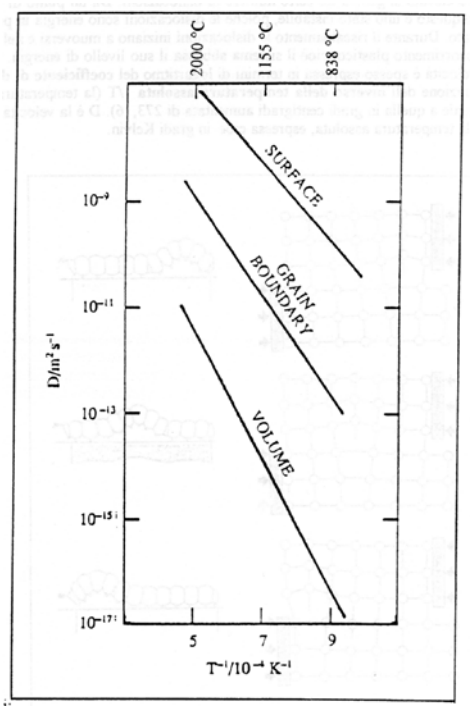

Figure 2. 4: Diffusion velocity

In the case of two particles in contact with each other through the flat surface of the sintering neck, a certain vacancies gradient between the highly curved surface of the particle and the adjacent flat surface exists, causing a vacancies flux from the neck region and the consequent movement of atoms into the neck region. [18]

The influencing variables on diffusion processes are temperature and time as well as the diffusion coefficients. For powder mixtures the sintering temperature may be above the melting point of the lower-melting constituent, so that sintering takes place also in the presence of a liquid phase. To avoid impairing of the component shape, it is of paramount importance a severe control over process parameters as heating rate, time, temperature and atmosphere.

2.1.4 Sintering atmosphere: Reduction of Metal Oxides

Controlled atmospheres are fundamental for almost all sintering processes, to prevent oxidation and enhance the reduction of existing surface oxides. From the previous considerations regarding the diffusion mechanisms which permit the consolidation of the component and the elimination of the porosity strongly correlated to the final impact and tensile strength of the PM-part, the presence of ceramic phases such as thick layer and particles of metal oxides on the surface reduces drastically the accomplishment of the densification due to their lower diffusion coefficient.

The usage of Chromium in the metallurgy industry has become significantly relevant due to its positive effects on properties of steel when alloyed. In addition to an improvement of mechanical and chemical properties, it is also relatively inexpensive and it can be recycled. However, the addition of Chromium to alloys means to control the more stable oxides which Chromium forms due to its high affinity for

oxygen. The main reaction which rules the reduction process in vacuum is:

$$\frac{2}{y}M_xO_y \rightleftharpoons \frac{2x}{y}M + O_2 \tag{2.4}$$

The standard Gibbs free-energy change ΔG^o, difference on the Gibbs free-energy of products and reactants in their reference state, indicates the trend of the reaction which proceeds spontaneously if the change is negative. The more negative is ΔG^o, the bigger is the equilibrium constant K.

$$\Delta G^o_{reaction} = \sum G^o_{products} - \sum G^o_{reactants} = -RTlnK \tag{2.5}$$

where R is the gas constant and T the temperature in Kelvin. The equilibrium constant K is function of products and reactants activity.

$$K = \frac{a^{\frac{2x}{y}}(M) \cdot a(O_2)}{a^{\frac{2}{y}}(M_xO_y)} \tag{2.6}$$

Considering that the activity of a solid phase can be assume equal to the unity, in this reaction K depends only on the partial pressure of oxygen (its activity).

$$K = p(O_2) = exp(\frac{-\Delta G^o}{RT}) \tag{2.7}$$

In presence of reducing agents such carbon and hydrogen, the other reduction reactions and processes occurring are listed as follows:

- Reduction by hydrogen:
$$\frac{2}{y}M_xO_y + 2H_2 \rightleftharpoons \frac{2x}{y}M + 2H_2O \tag{2.8}$$

- Direct carbothermal reduction:
$$\frac{2}{y}M_xO_y + 2C \rightleftharpoons \frac{2x}{y}M + 2CO \tag{2.9}$$

- Indirect carbothermal reduction:
$$\frac{2}{y}M_xO_y + 2CO \rightleftharpoons \frac{2x}{y}M + 2CO_2 \tag{2.10}$$

- Water gas reaction:
$$H_2 + CO_2 \rightleftharpoons H_2O + CO \tag{2.11}$$

Depending on the conditions of temperature, pressure or atmosphere, one reaction is preferably occurring with respect to the others.

The equilibrium constant of the reduction reaction by hydrogen is:

$$K = \frac{a^{\frac{2x}{y}}(M) \cdot a^2(H_2O)}{a^{\frac{2}{y}}(M_xO_y) \cdot a^2(H_2)} = \frac{p^2(H_2O)}{p^2(H_2)} \qquad \Rightarrow \qquad \frac{p(H_2O)}{p(H_2)} = exp(\frac{\Delta G_2^o}{2RT}) \tag{2.12}$$

where ΔG_2^o is the Gibbs energy difference for the reduction by hydrogen. Normally the quantity of water vapor is expressed in terms of dew point temperature, so that a tabular conversion from $p(H_2O)$ is required.

For indirect carbothermal reduction (2.10 the equilibrium constant is:

$$K = \frac{a^{\frac{2x}{y}}(M) \cdot a^2(CO_2)}{a^{\frac{2}{y}}(M_xO_y) \cdot a^2(CO)} = \frac{p^2(CO_2)}{p^2(CO)} \qquad \Rightarrow \qquad \frac{p(CO_2)}{p(CO)} = exp(\frac{\Delta G_3^o}{2RT}) \tag{2.13}$$

where ΔG_3^o is the Gibbs energy difference for the reduction by carbon monoxide[21].

The same analysis can be conducted for the water reaction 2.11 and the most meaningful consequence is that in a system containing both hydrogen and carbon monoxide as reducing agents, the partial pressures of the constituents cannot be changed independently from one another, since they are proportional through the equilibrium constant K of the reaction:

$$\frac{p(CO)}{p(CO_2)} = K \cdot \frac{p(H_2)}{p(H_2O)} \tag{2.14}$$

From calculations of Gibbs free-energy of metal oxides and using thermodynamic modeling softwares, data regarding the temperature dependence of both partial pressures ratios were collected into databases. One example is presented in Fig. 2. 5, provided by HSC Chemistry 7.0 database [21].

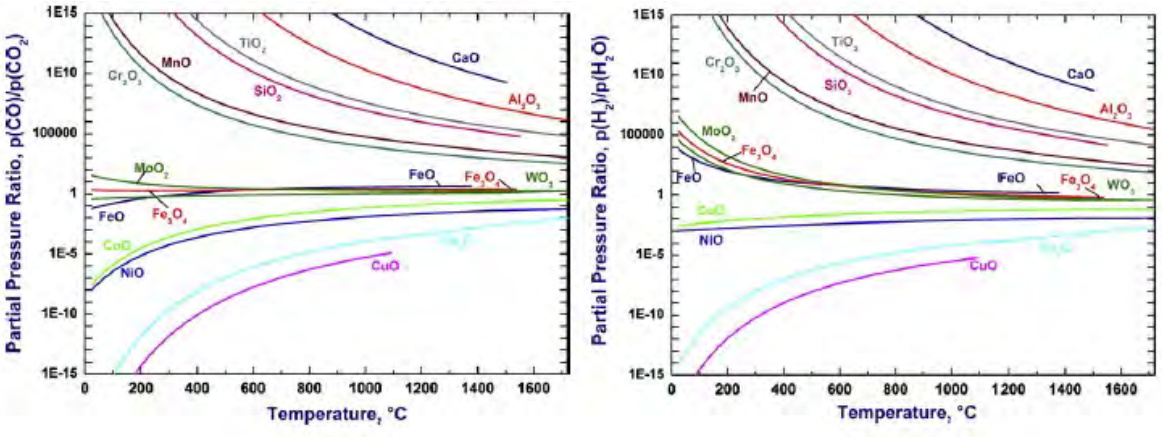

Figure 2. 5: Partial pressure ratios in equilibrium with some metal oxides

There are various atmospheres used in commercial applications. Pure hydrogen is limited because of cost and handling problems. Cracked ammonia represents a less expensive alternative but it should not be employed in applications where nitriding is an unwanted reaction.Exogas and endogas, produced by a careful controlled partial combustion of hydrocarbons, are very diffuse although such atmospheres

require special equipments. It is also possible to have a carburizing and simultaneously reducing atmosphere, from a combination of hydrogen and methane, for specific applications. Inert atmospheres like argon, helium and vacuum are very expensive and utilized in cases of sintering of high reactive metals including Titanium [18]. Despite the elevated cost of the vacuum atmosphere, its usage has notably grown for titanium alloys, hardmetals and high speed steels tools. In addition to a severe control of the sintering atmosphere, the thermodynamical stability of oxides is also of paramount importance. Previous studies [4-5] have shown that iron oxides can be easily reduced at low temperature (< 500 ℃) by Hydrogen according with the reaction 2.8 More stable oxides, such i.e. Chromium-based, require higher temperatures and the transportation of carbon via gas phase for carbothermal reduction, according with reactions 2.9, 2.10.

Ellingham-Richardson diagram

One way to visualize the stability of the oxide phase and predict at which temperature reduction can occur by the most appropriate reducing agent is to use the Ellingham-Richardson diagram. In this diagram, the Gibbs free-energy of metals and carbon oxidation is plotted against the temperature and the partial pressure of gases in reducing atmosphere analyzed above. From Fig. 2. 6, it is possible to estimate at which partial pressure of oxygen the oxidation reaction of a metal stops to be thermodynamically stable. On the other hand, it is clear that a decrease of pressure, e.g. vacuum condition, leads to a decrease of the minimum temperature necessary for avoiding oxidation and promoting reduction of oxides.

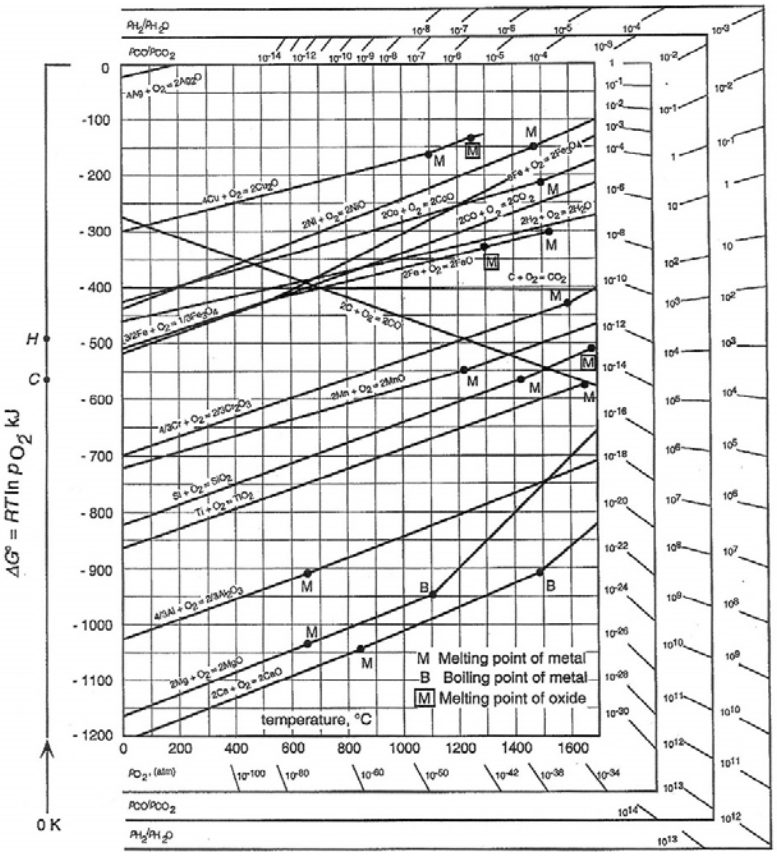

Figure 2. 6: Ellingham-Richardson Diagram for selected oxides

Furthermore, sintering in vacuum condition is convenient because dynamic vacuum creates a better mi-

croclimate since it sucks out gases produced by surface oxide dissociation and reduction (oxygen, carbon monoxide and carbon dioxide), that shifts both CO/CO_2 ratio and oxygen partial pressure to reducing conditions.

The estimation for instance of the necessary ratio of pressures CO/CO_2 at certain temperature is done by drawing a straight line from the letter C in the scale on the left side and pointed to the intersection of the isothermal line and the ΔG^o line corresponding to the specific oxide of interest. The extension of the resulting line to the $p(CO)/p(CO_2)$ scale on the right side gives the wanted value of the pressures ratio.

An other important information displayed in this diagram is the existing intersection point between the ΔG^olines characterizing the two oxidation reactions of carbon.

$$C + O_2 \rightarrow CO_2 \qquad \Delta G^o = \Delta H^o \tag{2.15}$$

in the case of carbon oxidation to carbon dioxide, the system does not exhibit an entropy change with an increase of the temperature so that the Gibbs free-energy is constant, according to
$\Delta G = \Delta H - T\Delta S$.

$$2C + O_2 \rightarrow 2CO \qquad \Delta G^o \neq \Delta H^o \tag{2.16}$$

For the second reaction, the entropy of the system sensibly increases resulting in lower Gibbs free-energy at higher temperatures. This means that by heating above the temperature equilibrium of the total reaction $C + CO_2 \rightleftharpoons 2CO$ [Boudouard equilibrium] carbon monoxide is more stable than CO_2 and has a higher reducing activity. In addition to that, the dissolution of CO to CO_2 at lower temperatures is hindered due to kinetic reasons thus the stability field of carbon monoxide starts below the theoretic temperature of the Boudouard equilibrium.

2.2 Diffusion alloying method for the production of Cold Work tool Steels [CWS]

In the field of powder forging of carbon-rich steel parts, the addition of carbon in form of graphite to the iron powder, instead of pre-alloying it, has been shown to be more effective since it increases the pressability of the powder, acting as lubricant, and increases its strength and hardness. During sintering, in fact, graphite dissolves and carburizes the steel powder. Carbide-rich cold work tool steels feature a multiphase microstructure with hard and brittle carbides embedded in a tough metallic matrix. The efficiency of carbides on wear and abrasion resistance depends on different factors. At first instance, the carbides must be harder than the abrasive material and their size must be similar to the wear groove. Furthermore, a minimal free matrix length between carbides is preferable to prevent cold welding and enhance toughness. Therefore, carbide grain size and dispersion are critical and need to be controlled. While ingot metallurgy leads to the formation of an unwanted carbide size or network structure deteriorating mechanical properties, the route via pre-alloyed powder metallurgy for the formation of material featuring high-melting carbides such as NbC, TiC and VC is impeded as well due to the known problem of primarily precipitation of carbides from the melt which do subsequently clog the nuzzle during atomization. Thus, again, the atomization of pre-alloyed carbon-free melt rich on carbide forming elements and the subsequently addition of graphite to iron-based powders is advantageous. During hot isostatic pressing the graphite dissolves and leads to the precipitation of a very finely dispersed carbides. Previous studies indicate that carbide size depends strongly on pressure and also weakly on temperature. It has also been found out that transport of carbon necessary during carburization is based not only on diffusion of carbon in the solid lattice but also the presence of gaseous products formed during reduction process is required for the carburization[4].

2.2.1 Niobium-rich CWS

In order to preserve a necessary amount of Chromium in the metallic lattice for corrosion resistance, elements with higher affinity to carbon than Chromium can be added. Niobium and Vanadium form super hard MC-type carbides, the difference between these two is that the solubility for Chromium into carbides is higher in case of VC; instead, NbC remains relatively pure. Previous investigations [1-2] were conducted for producing high Nb ($> 8\%$) stainless cold work steels. It has been shown that, starting from a melt containing 9%Nb, 12%Cr, 2%Mo and atomized in a nitrogen gas stream, was

possible to obtain dispersed Nb-carbides even at very high (2.8%) carbon contents admixed. Increasing progressively the carbon content from 0 to 2.8%, no graphite phase or carbides network have been observed. Concerning the size and the distribution of the NbC in alloys based on the 9%Nb powder, a difference exists for alloys containing less and more than 1%C. At <1%C, the distribution of carbides is not uniform as carbon forms carbides close to the surface and not diffusing deep into the grain. This can be explained due to the difference on diffusivities of carbon and niobium. Carbon is an interstitial element and it diffuses faster in the metallic lattice than niobium, since the latter is a substitutional diffusion element. For carbon concentration higher than 1%, it has been observed that the size of carbides is much smaller. The main explanation for this phenomenon can be found from the assumption that Boudouard equilibrium is established promoting fast carbon transport via gas phase such CO. If diffusion rate of carbon is slow, Laves phase can eventually spheroidize and grow, leading to a bigger size of carbides precipitating at its boundaries [1]. This and other previous studies, show again that diffusion plays a key-role before and during sintering for the obtaining of desired microstructure. In this scenario, oxides reduction is also important because oxide phase can act as a barrier for carbon-uptake and provide gaseous atmosphere with CO, necessary for the carburization. Recent attempts are directed to the replacement of niobium carbides with titanium or vanadium carbides.

Chapter 3

Aims and way

As it was mentioned above, this thesis deals with the analysis of the carbothermal reduction of metal oxides on powder surface, replicating suitable conditions for sintering and the In-Situ formation of carbides.

Chapter 2 indicates carbon monoxide as the most effective reducing agent due to the constant decrease of the Gibbs free-energy with the increase of the temperature. Therefore it would be reasonable concluding that the complete reduction of oxides can be achieved with the addition of higher percentages of graphite, followed by the subsequent formation of carbides leading to the improvement of PM parts properties. To investigate this, different percentages of additional carbon in the form of graphite are manually added to the three types of powders.
In the thesis the data provided by the RGA experiments, in particular way the value of partial pressure of the principal gases developed in the reduction reactions, will be evaluated to find the temperature regions where the oxides involved are reduced. Additionally SEM and EDS will be conducted to analyze the powders surface after heat treatment with different graphite addition. The EDX is used to measure the composition of the surface particulates to find out if the oxides are reduced and the carbides are formed.

The formation of interparticle connections and the distribution of particulates are observed with SEM microscope as well.

Chapter 4

Experimental

4.1 Materials and Laboratory Instruments

4.1.1 Powders

In the table 4. 1 the chemical composition of the three powders used is reported.

Alloy	Fe	C	Cr	Ni	Si	Mn	Mo	Ti	Al	V
GuiCr	81,12	0,16	15,57	0,52	1,02	0,52	0,6	–	0,04	–
PSHTi	79,91	0,09	13,81	–	–	–	1,1	5,09	–	–
GuiV	74,88	0,37	17,08	–	–	–	0,66	–	–	7,02

Table 4. 1: Powders under investigations

The GuiCr powder is mostly an Iron and Chromium-based steel with several additional elements alloyed such Silicon, Manganese, Aluminum and Nickel. The addition of Si in alloy leads to an increase of strength whereas the presence of Mn guarantees an increase of hardenability by reducing the critical cooling rate.

GuiV features with respect to the GuiCr an higher amount of Chromium and a relevant percentages of Vanadium. Vanadium is an alloying element with an high affinity for oxygen and it is also a strong carbides forming alloying element.

PSHTi features the lower amount of Chromium but a significant percentage of Titanium. Titanium is also a strong carbides forming element with such affinity for oxygen to require atomization with nitrogen stream in controlled atmosphere.

The percentages of carbon taken into account are: 0%, 0,3%, 1,5% and 2%.

4.1.2 Residual Gas Analyzer (RGA)

A Residual Gas Analyzer (RGA) consents to measure the gases present in a low-pressure environment. The experimental data, elaborated by the machine and analyzed with proprietary software, is given as partial pressure of the gases developed under vacuum condition. In this case RGA was used to detect molecules evolving from the sample during heating process, obtaining information about chemical reaction taking place.

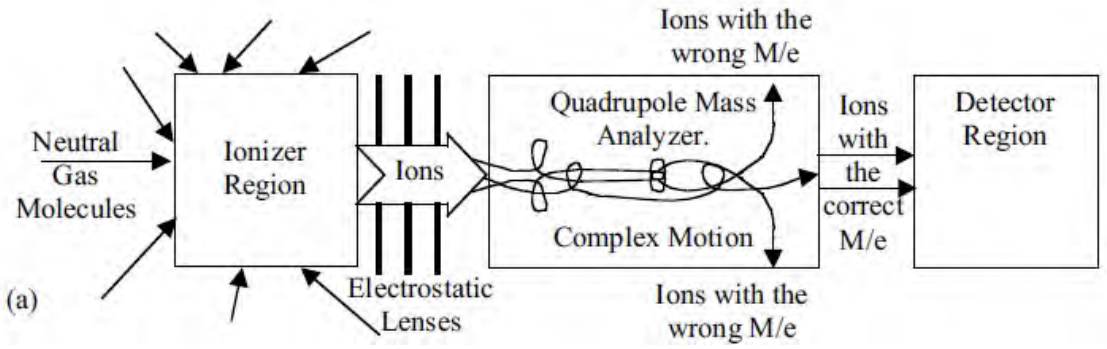

Figure 4. 1: Operating Diagram of Residual Gas Analyzer

The scheme of the whole process can be seen in Fig. 4. 1. At the first step, an ionizer unit converts many neutral gas molecules into positive ions in a well-controlled region at a specified electric potential. The ionization of molecules occurs due to the thermionic emission of electrons from a filament wire supplied with current. The power supply unit provides this current and the thermionic emission process becomes more intensive with the increase of the temperature of the wire by Joule effect, allowing more electrons to escape from the metal lattice to the vacuum. The electrons are subsequently accelerated by a potential difference, colliding next with molecules. The energy required to ionize molecules is transferred from electrons during collisions.

These ions are afterwards accelerated by a series of electrostatic lenses and formed into a beam. The ion beam is subsequently passed into the quadrupole mass analyzer region which acts as a filter. In this region specific fields detect selected mass to charge ratio (M/e) ions, separating them from other ions which are subsequently neutralized becoming undetectable.

Once specific M/e ions have been passed through the filter, the final step consists on detecting and counting the ions. In RGA systems, two methods are mostly used: a simple electric structure based on a "Faraday cup" or an advanced amplifier technology called "Electron Multiplier". The RGA system in use in the laboratory is a type E-Vision (MKS Instruments) based on a Faraday cup structure. This structure elaborates a partial current signal (I) of ions flowing through the Faraday cup. Since the

definition of current as the net flow of ions passing through a surface, the magnitude of this current is directly correlated to the total amount of specific M/e ions and thus is the partial pressure of the molecules with mass M. The software elaborates the electrical current into a pressure expressed in mbar.

In the case of detected mass 28 amu two different molecules contribute to the formation of the signal: molecular nitrogen (N_2) and carbon monoxide (CO). The main difference and the way to predict which molecule has more effect on the signal come observing the total spectrum of (N_2) and (CO). Whereas (N_2) produces peaks at 28 amu and 14 amu (N), the latter produces peaks at 28 (CO), 12 (C) and 16 amu (O). It is moreover reasonable possible that CO molecule can break during the high energy ionization, therefore an analysis of partial pressure of atomic carbon and oxygen is suggested. [13]

4.1.3 SEM and EDX

Compared to the light microscopy, which is based on light photons scanning the surface of the object, the Scanning Electron Microscopy uses a high energy electrons beam which scans the surface of the sample. The production of the images is the result of the way interaction of the beam with the specimen, which can occur in different modalities so that several elaborated signals define topography and composition of the surface. The main improvements gained with the implementation of this technology essentially are higher resolution, reached of about nanometers, and depth sharpness. The microscope is formed by two parts: the electronic console and the electrons column. The console allows the operator to interact with switches and knobs for adjustments such as focus, brightness and filament current. The electrons column [Fig. 4. 2] is where the beam is generated under vacuum and focused on the specimen generally through electromagnetic deflection coils. The electrons are emitted in the Electron Gun unit from a tungsten filament by thermionic process at high temperatures and accelerated towards an anode in consequence of a potential difference. The beam is now converged by the actions of condenser lenses which reduce the size of the beam down to 1000 times. Apertures in the column may intervene

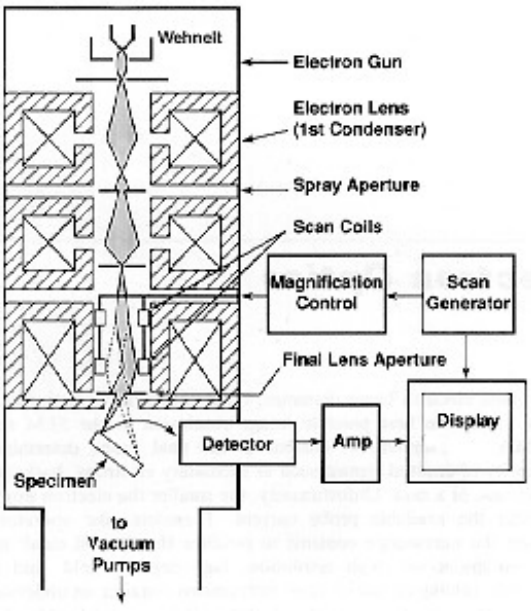

Figure 4. 2: Electron column diagram

to adjust the size of the hit spot on the surface, determining the resolution and the depth. In the lower portion of the microscope, the sample chamber and the detector of secondary electrons are placed. The analysis occurs when a vacuum condition is reached in the sample chamber, to avoid interactions of the electron beam with air molecules.

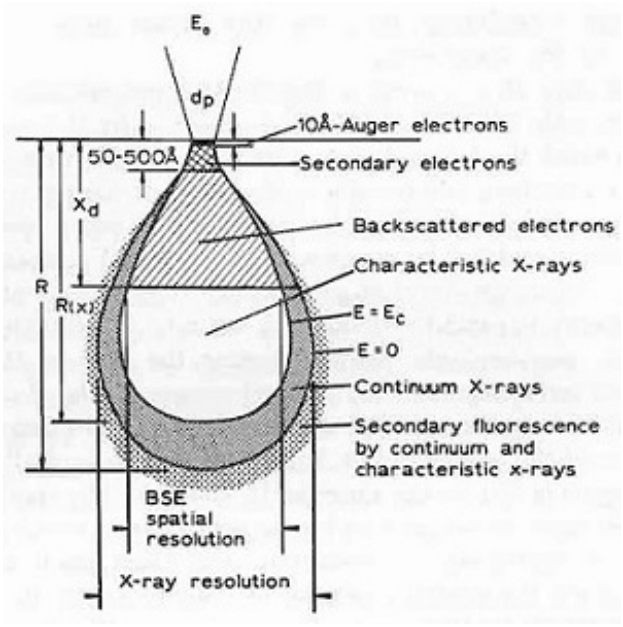

Figure 4. 3: Electron beam-Specimen

The visual inspection of the surface takes place due to the signals given by secondary and backscattered electrons. Secondary electrons (SE) are the result of the inelastic scattering collisions which eject electrons from the electronic k-shell of the specimen's atoms, revealing the surface structure of the material. Because of low energy of these electrons, they must be produced only from the top few nanometers thickness of the specimen

Backscattered electrons (BSE) are instead originated from high energy electrons of the beam which are reflected out of the specimen interaction volume in consequence of elastic collisions with the surface atoms. Since atoms can backscatter differently incident electrons, depending on their atomic number and displayed with different brightness, this signal provides contrast information between areas with different chemical compositions.

An other possible source of information for characterizing the surface is the X-ray signal. This signal is obtained when the electron beam may excite an electron near the nucleus, ejecting it from the shell and creating an electron hole. An electron of the higher energy outer shell then fills the hole and the difference in energy between the two shells is emitted in form of a X-ray. Since the X-ray photon is characteristic for the atom, the Energy-dispersive X-ray (EDX) analysis offers with the spectrum obtained a chemical characterization of a small area of the sample, although it is not possible to determine directly the chemical formula of the species. [19-20] The SEM model used and available in the laboratory is type LO 1540 VP.

4.2 Methodology

At first instance, attentions were placed on the preparation of the crucibles containing the powder during the RGA experiments. The first step consisted on cutting the crucibles providing them the characteristic shape shown in figure 4. 4 beside, with 5.1 mm inner diameter and a height of 20 mm. The crucibles were afterwards cleaned inside an ultrasound cleaner tank immersed in ethanol solution for 20 minutes, with an intermediate change of the solution. The crucibles were subsequently dried under an hot air stream in order to evaporate completely the ethanol solution and put into a plastic bag.

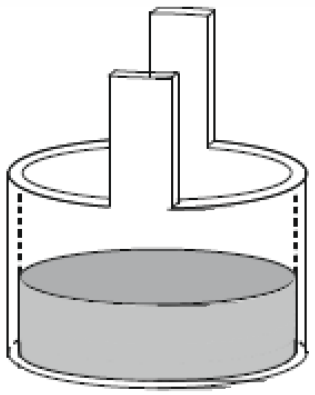

Figure 4. 4: Alumina Crucible

To eliminate every residual of previous experiments or contaminating substances, two crucibles at once were allocated into the vertical dilatometer type Linseis L75PT (equipped with the E-Vision type residual gas analyzer), performing a baking process at high vacuum condition. In this process no dilatometric or RGA data were obtained, the device was used only as a furnace. When the pressure value of $2 \cdot 10^{-4}$mbar was reached and through the software the dilatometer was equipped with, the parameters of the process were set as follows:

- Heating rate = 10K/min
- Tmax = 1300 ℃
- Holding time = 3 h
- Cooling rate = 20K/min

Regarding the preparation of powders, the right amount in weight of carbon as graphite was added to the steel powders in controlled atmosphere of nitrogen and the mixtures were subsequently mixed for 30 minutes. For each powder, one RGA experiment was conducted with the same following methodology.

the crucible was weighed and filled with around 0.8 ÷0.9 g of powder. The specimen was afterwards inserted in the vertical dilatometer acting as furnace and the vacuum was created through the usage of magnetic and turbo-molecular pumps.

Once that the value of pressure ($2 \cdot 10^{-4}$mbar) was reached, with an intermediate cleaning ventilation of the furnace's camera with helium, the residual gas analysis was activated simultaneously with

the start of the heat treatment process set with the following parameters:

- Heating rate = 5K/min
- Tmax = 1250 ℃
- Holding time = 15 min
- Cooling rate = 10K/min

The RGA data was exported as text file using the proprietary software provided by MKS and elaborated with ®Origin. Taking into account the thermal inertia of the dilatometer, the heating rate is not constant at the beginning of the heat treatment process, determining its dependency with time. The system reaches the condition of stationary state after ∼30 minutes, when the temperature value is ∼200 ℃ .

However, a linear approximation can be assumed for the evaluation of temperature values under ∼200 ℃ as out of the investigating interest. The sensitivity of the temperature's measurements from the instrument is $5 \cdot 10^{-3}$ ℃ and the measurement occurred each second.

The specimen's surface of each powder with 0% and 1.5% of carbon added was examined with SEM microscope and EDX.

Chapter 5

Results

In this chapter the examination of the RGA data and the characterization of the specimen's surface with the SEM microscope are reported. For each measurement, are given the general graph showing the slope of the principal gases involved and a rescaled-plot without the partial pressure of mass 28 amu, indicating CO and N_2.

5.1 GuiCr Powder

5.1.1 GuiCr without additional graphite

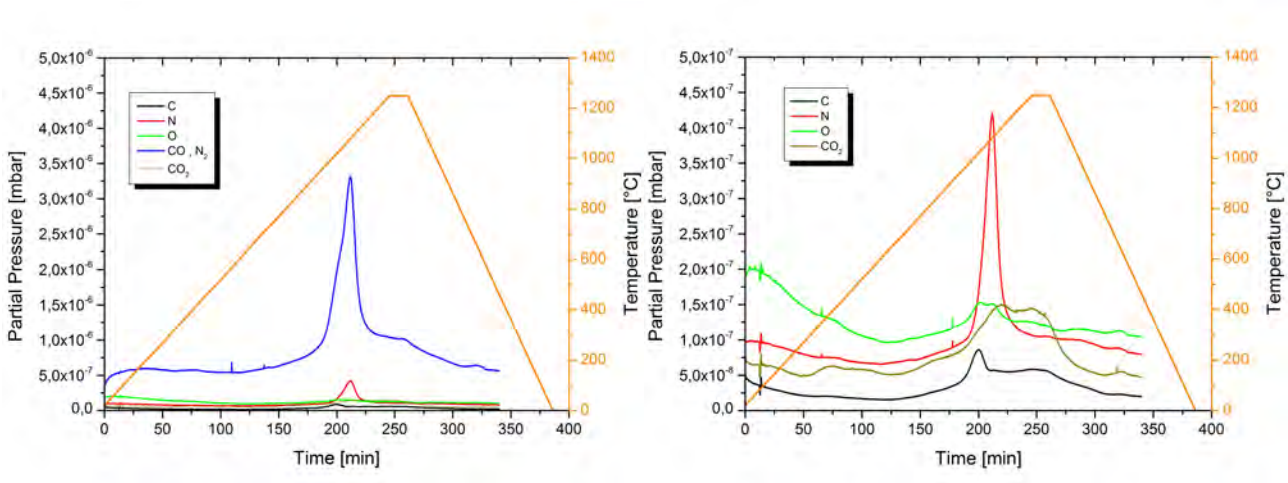

(a) General plot

(b) Rescaled

Figure 5.1: RGA experimental data for GuiCr powder with 0% of Carbon added

Comparing Figs. 5.1a and 5.1b shows that a sensible increase of the partial pressure of all masses occurs at ∼700 ℃ with a secondly remarkable change of slope at ∼950 ℃ .

It is also visible a similar behavior in case of masses 12, 14 and 44 as a principal peak is limited by the presence of a plateau at higher values of partial pressure with respect to the first half of the heating process. For mass 14, 28 and 44 (less pronounced) the maximal pressure is measured at ∼1080 °C whereas the peak of carbon is anticipated at the temperature of 1000 °C . The end of the plateau and the consequent decrease of the pressure correspond with the beginning of the cooling process. This is more evident for carbon, carbon monoxide and carbon dioxide.

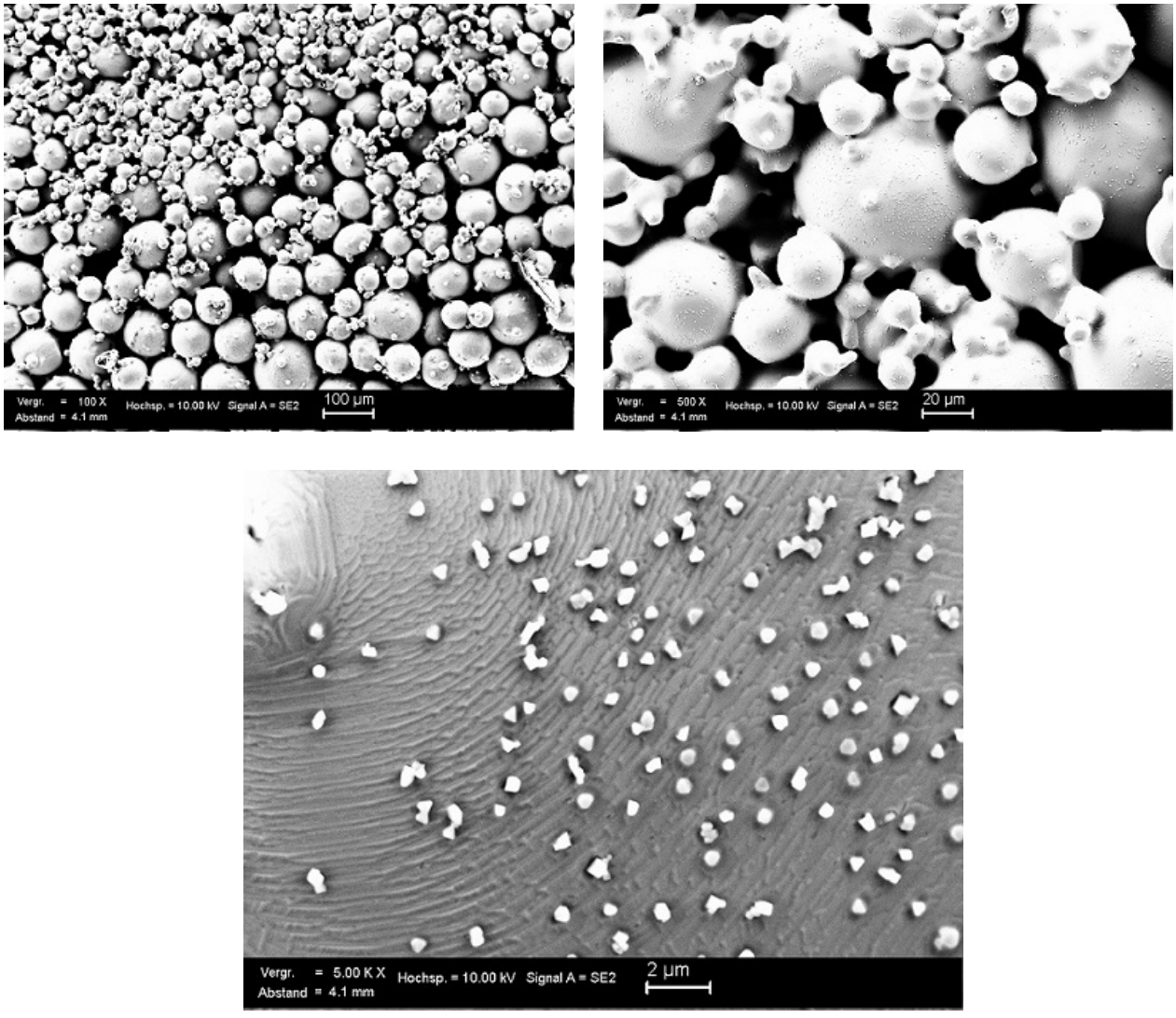

Figure 5. 2: SEM analysis of GuiCr samples surface without addition of graphite

Fig. 5. 2 shows the analysis of specimen's surface conducted with the Electronic Scanning Microscope. In the case of GuiCr powder without graphite admixed, can be seen through a 100x enlargement that strong interparticles connections such sintering neck are not evident. Increasing the enlargement at 1000x and 5000x, concentric grooves and brighter masses of 1μm diameter size can be found. As

reported in table 5.1 below, two EDX analysis indicates that the surface of the biggest particle is mostly composed by iron and chromium whereas spotting on the brighter masses a bigger amount of oxygen was detected (table 5.2).

Measurement 1			Measurement 2		
Element	Wt%	At%	Element	Wt%	At%
C K	1.09	4.45	C K	0.87	3.54
O K	3.12	9.61	O K	3.39	10.33
FeL	72.63	64.02	FeL	63.26	55.21
CrK	23.16	21.93	CrK	31.87	29.88
–	–	–	SiK	0.60	1.05
Total	100	100	Total	100	100

Table 5.1: EDX on surface

Measurement 1			Measurement 2		
Element	Wt%	At%	Element	Wt%	At%
C K	0.74	2.92	O K	13.02	32.62
O K	5.36	15.91	FeL	30.25	21.71
FeL	63.77	54.26	AlK	2.65	3.93
CrK	28.65	26.18	CrK	31.07	23.95
MoL	1.48	0.73	SiK	1.44	2.05
–	–	–	MnK	21.57	15.73
Total	100	100	Total	100	100

Table 5.2: EDX on particles

Complete spectrum of all EDX measurements are provided in the appendix.

5.1.2 GuiCr with 0,3% of additional carbon admixed

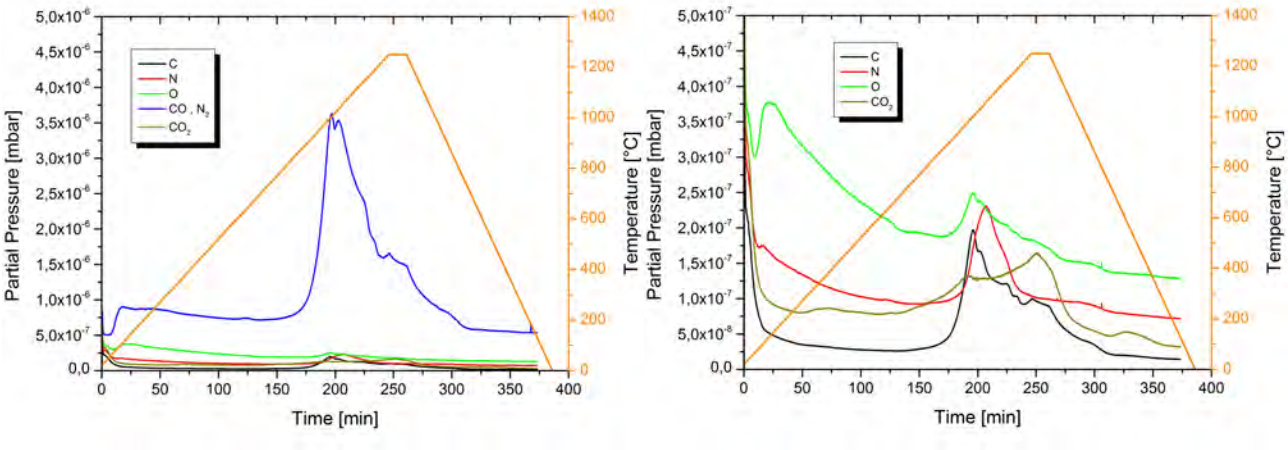

(a) General plot

(b) Rescaled

Figure 5.3: RGA experimental data for GuiCr powder with 0,3% of Carbon added

After admixing additional 0,3% of graphite, Fig. 5.3 illustrates a sensible change on general behavior. Mass 12 (C), 16 (O) and 28 (CO) show at the same range of temperature from 950 °C to 1050 °C a principal peak followed by an other less pronounced peak. From the previous considerations mentioned in the section 4.1.2, this indicates an evolution of CO instead a measurement of molecular nitrogen. Increasing the temperature till the value of 1200 °C , the partial pressure of these masses features

a progressive decrease which ends at the temperature of 1200 °C where an other smaller peak is detected at the beginning of the cooling process. Partial pressure of CO_2, instead, presents an increase of the values with a smaller peak at the same temperature range previously mentioned and another more consistent peak at the beginning of the cooling process. The spectrum of mass 14 (N) displays the same characteristic unique peak at ∼1080 ℃ .

5.1.3 GuiCr with 1,5% of additional carbon admixed

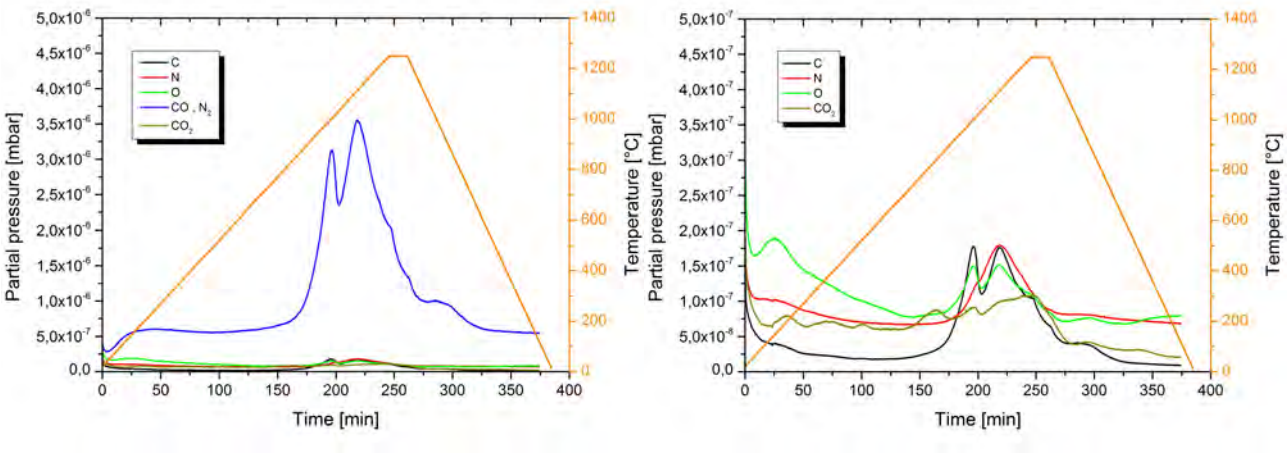

(a) General plot (b) Rescaled

Figure 5. 4: RGA experimental data for GuiCr powder with 1,5% of Carbon added

Fig. 5. 4 reports the data acquired from RGA experiment conducted on GuiCr with additional 1,5% in weight of graphite. With respect to the previous observation, the curves of the partial pressure feature a slightly change on tendency since a more sensible distinction of the two peaks can be noticed. For masses 12, 16 and 28 the first peak remains with the maximal value at the temperature of ∼1000 ℃ whereas the second and larger peak is shown at 1100 ℃ (at which the maximal pressure of the mass 14 is also reached).

In case of carbon and oxygen cannot be noticed a difference of intensity between the two peaks. Considering moreover the peak of atomic nitrogen, it can be deducted that the peak at 1100 ℃ is formed by carbon monoxide and molecular nitrogen.

Regarding the partial pressure of carbon dioxide, can be seen the same not intense peak at ∼1250 ℃ .

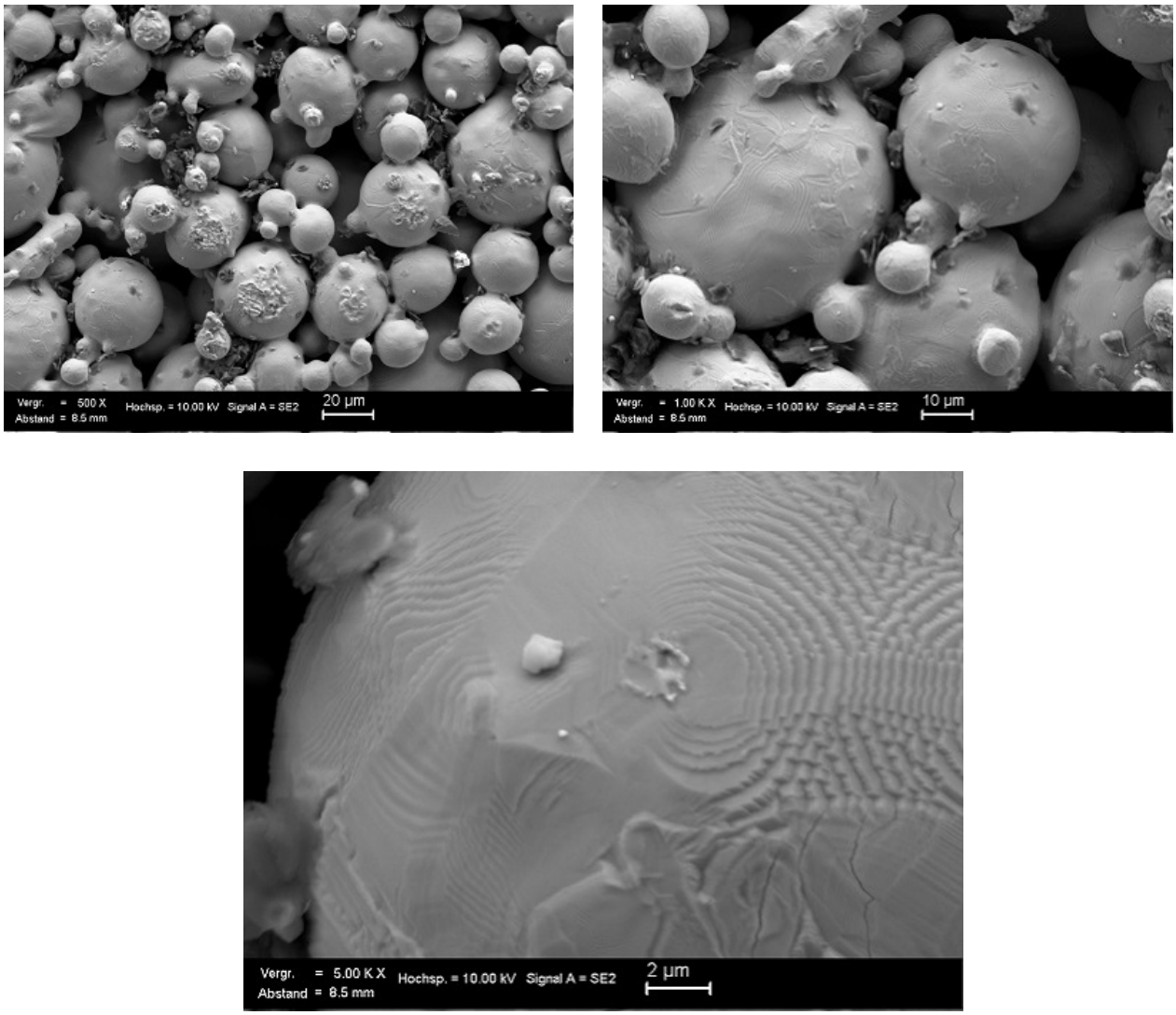

Figure 5. 5: SEM analysis of GuiCr samples surface without addition of graphite

Fig. 5. 5 presents observations on particles surface and it can be noticed that sintering necks are visible. Table 5. 3 reports the composition of the clean surface and the composition of the grooves which can be noticed in the picture with the major enlargement. Both measurements reveal presence of carbon and oxygen although the surface remains mostly based on iron.

As can be seen in table 5. 4 in the bright particles the content of carbon and oxygen is higher and cannot be noticed a remarkable increase of chromium content.

Surface			Grooves		
Element	Wt%	At%	Element	Wt%	At%
C K	2.81	10.88	C K	1.35	5.53
O K	3.62	10.51	O K	3.39	10.11
FeL	73.06	60.84	FeL	81.01	71.21
CrK	18.15	16.24	CrK	13.25	12.51
MnK	1.09	0.92	MnK	0.21	0.19
MoL	1.27	0.62	MoL	0.89	0.45
Total	100	100	Total	100	100

Table 5.3: EDX on surface

Measurement 1			Measurement 2		
Element	Wt%	At%	Element	Wt%	At%
C K	4.52	15.11	C K	9.77	30.57
O K	8.94	22.43	O K	4.60	10.82
FeL	76.45	54.95	FeL	66.27	44.61
CrK	9.32	7.20	CrK	19.36	14.00
MoL	0.76	0.32	MoL	-	-
Total	100	100	Total	100	100

Table 5.4: EDX on particles

5.1.4 GuiCr with 2% of additional carbon admixed

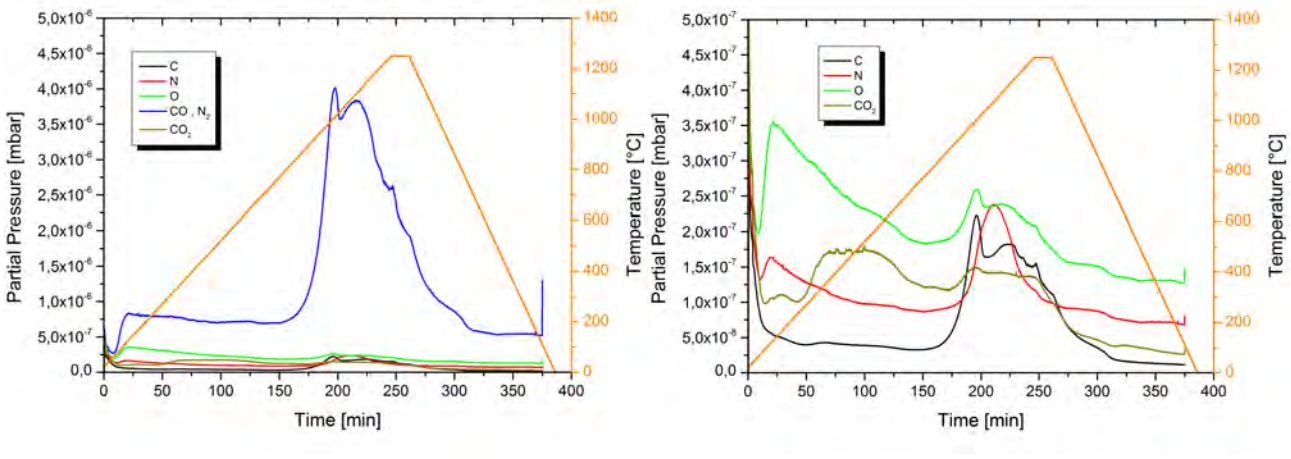

(a) General plot

(b) Rescaled

Figure 5.6: RGA experimental data for GuiCr powder with 2% of Carbon added

Consecutively the addition of 2% of graphite to GuiCr powder, can be seen in Fig. 5.6a that the maximal pressure of the first peak registered for mass 28 is confirmed to be at 1000 ℃ but with higher value compared to the case of GuiCr with 0,3% of carbon. Is also given in the two graphs a larger second peak in the case of mass 28 and more evident for masses 12 and 16. Although also an higher amount of atomic nitrogen is detected after the temperature corresponding with the top of its peak, the related increase of the second peak for carbon, oxygen and carbon monoxide may indicate an higher evolution of CO in the temperature range until the maximum temperature of the heating process. Furthermore, can be found a change on carbon dioxide's behavior since the value pressure is approximately constant after the temperature value of 1000 ℃ .

5.2 PSHTi Powder

This section deals with the presentation of the results obtained by measurements conducted on the powder rich on Titanium.
As it can be noticed in the following graphs, the same scale of the partial pressure used for presenting the previous results is maintained despite the different values. This intends to give a first comparison between different powders which will be discussed in details in the next chapter.

5.2.1 PSHTi without additional graphite

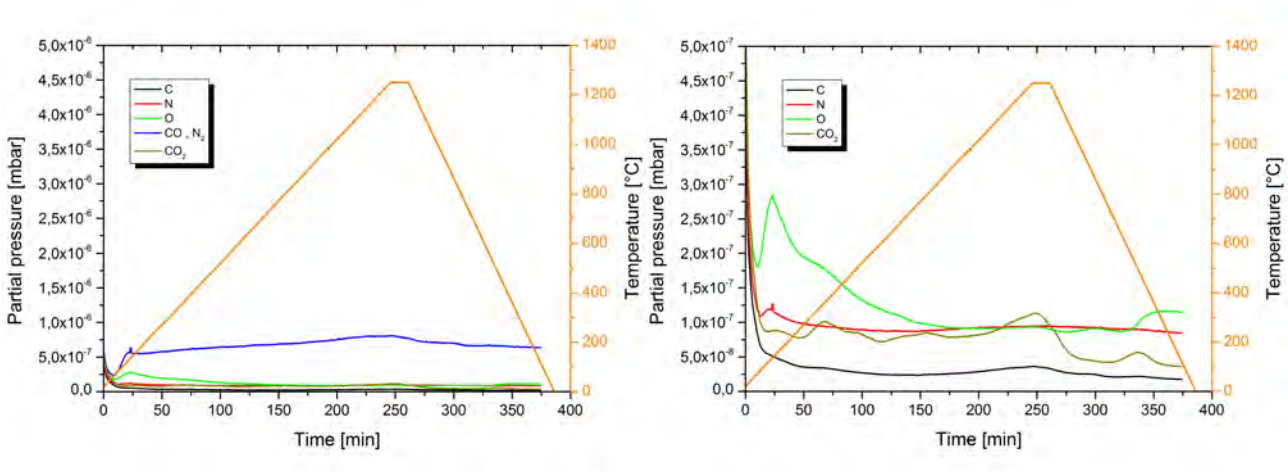

(a) General plot (b) Rescaled

Figure 5. 7: RGA experimental data for PSHTi powder with 0% of Carbon added

Fig. 5. 7 summarizes the partial pressure of the principal gases evolved during the heat treatment process performed on titanium-rich powder's specimen in vacuum atmosphere. Regarding the mass 28, can be seen the characteristic initial strong increase of the partial pressure at the beginning of the heating process ($< 150\,℃$), evident in every measurement conducted, and a subsequent feeble and constant rise of pressure until the beginning of the holding time at $1250\,℃$. The same tendency can be observed in Fig. 5. 7b for mass 12 (C), whereas at maximal temperature carbon dioxide presents a more consistent peak with a pronounced next decrease of pressure. In the case of mass 16 (O), a peak is visible from $100\,℃$ to $300\,℃$, followed by a progressive decrease of pressure values.

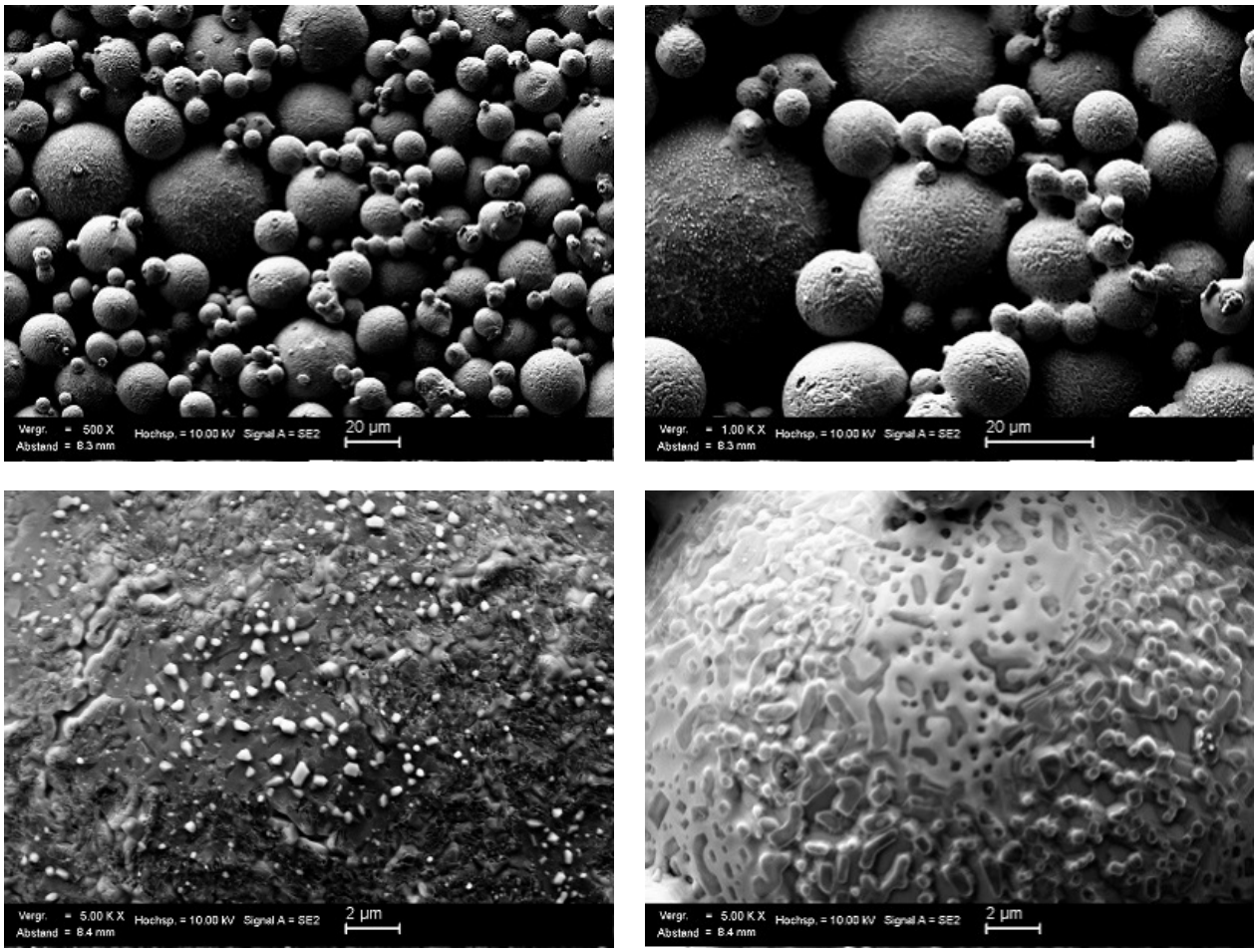

(a) First environment (b) Second environment

Figure 5. 8: SEM analysis of PSHTi samples surface without addition of graphite

Analysis with SEM on specimen's surface produced with PSHTi powder without the additional graphite admixed shows through 500x and 1000x enlargements that a big dispersion of particles sizes is present. Can also be noticed that sintering necks connect only small particles whereas big particles shows no interconnections. Observing furthermore the surface of the big particles two different environments are reported. The first environment, which can be seen on the particles on the left and maximized in Fig. 5. 8a, features: brighter small particles of 0,5μm average diameter , darker small spots and a grey-scale surface. Table 5. 5 illustrates the EDX analysis on these three components respectively reported. The second environment, found on the surface of the center particle and detailed in Fig. 5. 8b, consists on parts in relief delimited by bright edges, isolated darker spots and a below surface. Compositions are displayed in tables 5. 5. Can be noticed that an unexpected relevant amount of carbon is present in almost all the measurements.

	bright part.		dark spots		surface	
Element	Wt%	At%	Wt%	At%	Wt%	At%
C K	2.49	9.41	6.45	18.11	6.44	17.93
O K	3.85	10.90	12.56	26.49	13.33	27.88
FeL	63.06	51.20	12.90	7.80	15.34	9.20
CrK	5.31	4.63	3.28	2.13	2.92	1.88
TiK	25.12	23.78	64.30	45.29	61.44	42.93
MoL	0.17	0.08	0.51	0.18	0.54	0.19
Total	100	100	100	100	100	100

Table 5. 5: First environment

	part. in relief		dark spots		surface	
Element	Wt%	At%	Wt%	At%	Wt%	At%
C K	0.95	3.98	6.20	20.15	3.14	11.32
O K	2.83	8.87	5.30	12.93	4.81	13.04
FeL	71.63	64.34	30.91	21.60	50.75	39.41
CrK	12.97	12.51	8.10	6.08	9.60	8.01
TiK	8.06	8.44	46.85	38.17	30.65	27.75
MoL	3.55	1.86	2.65	1.08	1.06	0.48
Total	100	100	100	100	100	100

Table 5. 6: Second environment

The EDX analysis offers different scanning options. The electron beam can be pointed on a spot, a small area or it can scan the surface along a line. The last option can be useful for verifying the variation of the elements content for instance inside and around a particle.

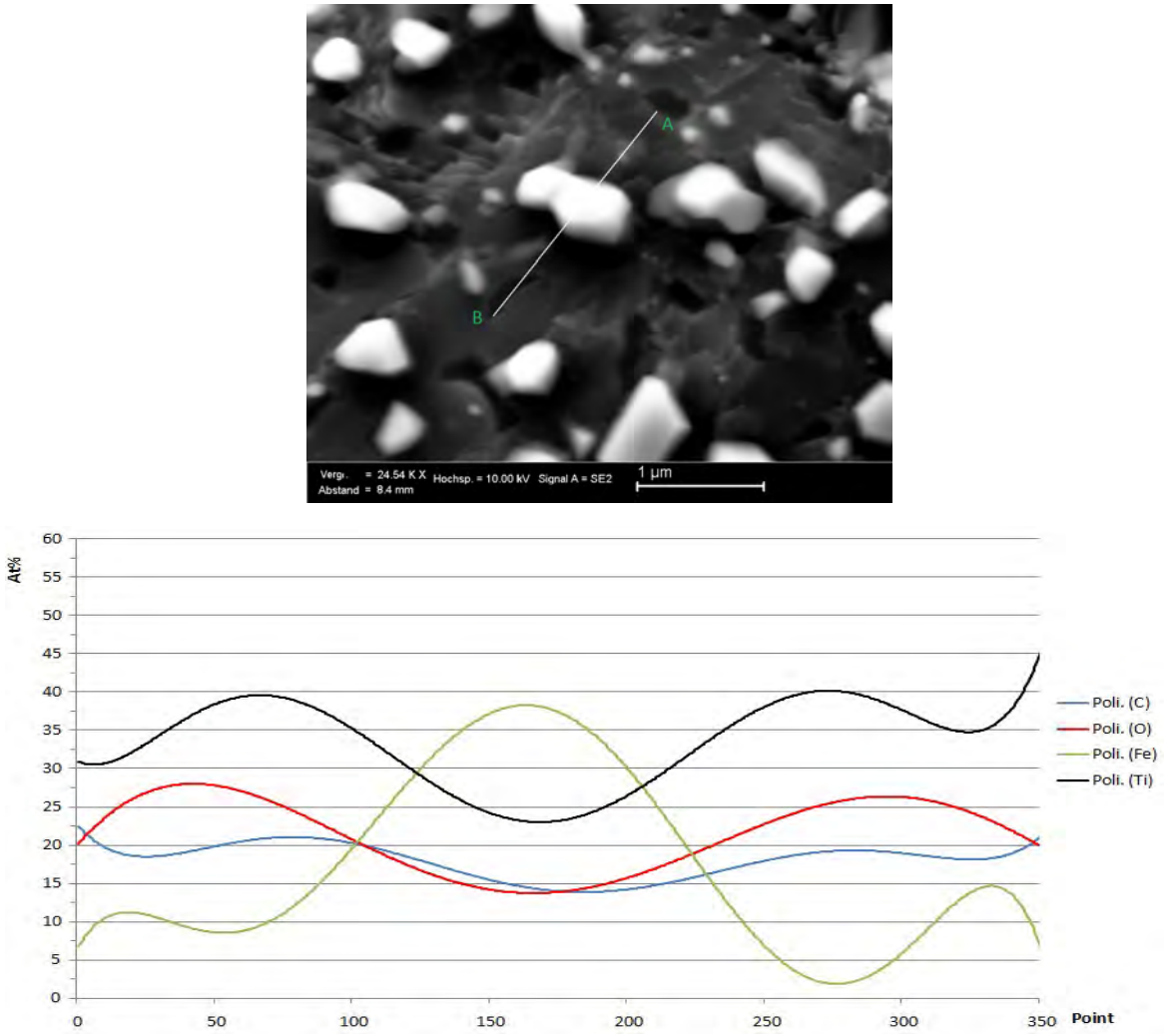

Figure 5. 9: EDX line analysis conducted on the bright particle

A bright particle found previously in the first environment was scanned along the white line visible in Fig. 5. 9 from the A point to B point. 352 EDX measurements were conducted along the line, generating the same number of spectra. Due to the high quantity of data for the elements Ti, C, O and Fe and its difficult elaboration caused by the sensible variation of the content point to point, it was chosen to display the analysis with the usage of the tendence line with the higher order provided by the software to fit with more accuracy possible the data.
Strangely no data regarding chromium have been acquired. However, it can interestedly be seen that in the bright particle, corresponding at the middle part of the points values, an enrichment of iron with a simultaneously decrease of C,O and Ti contents is evident, whereas around the particle titanium and oxygen contents gather more than carbon.

5.2.2 PSHTi with 0,3% of additional carbon admixed

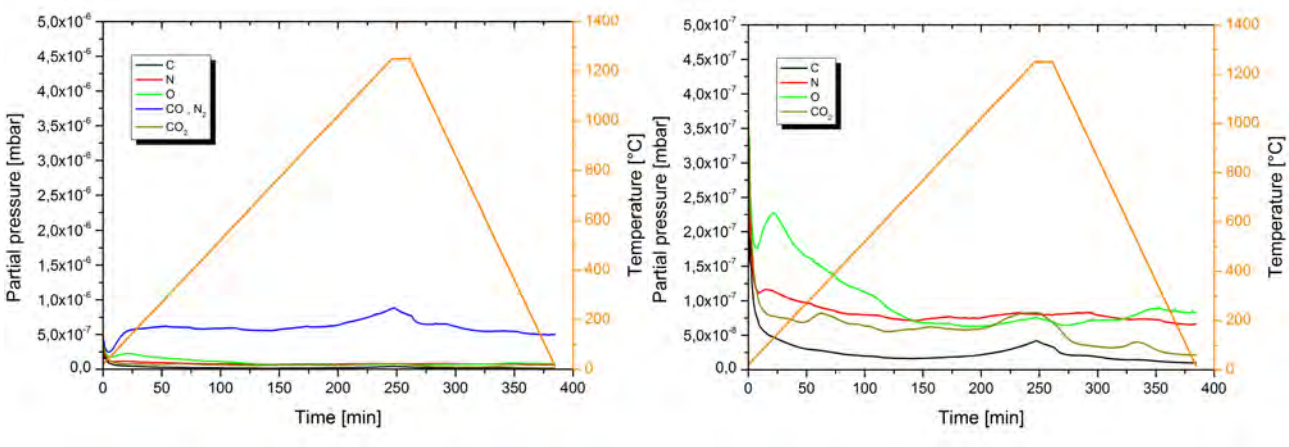

(a) General plot (b) Rescaled

Figure 5. 10: RGA experimental data for PSHTi powder with 0,3% of Carbon added

As evident from Fig.s 5. 10a and 5. 10b the partial pressure of mass 12 and mass 28 shows the same tendency with one weak peak and one sensible change of slope at the same temperature of 1250 ℃ and at the end of the holding time, respectively. This tendency is not noticeable for mass 14, which features a mostly constant value of pressure measured and for mass 44, which presents a large but not intense peak from the temperature of ∼1100 ℃ to the beginning of the cooling process.

5.2.3 PSHTi with 1,5% of additional carbon admixed

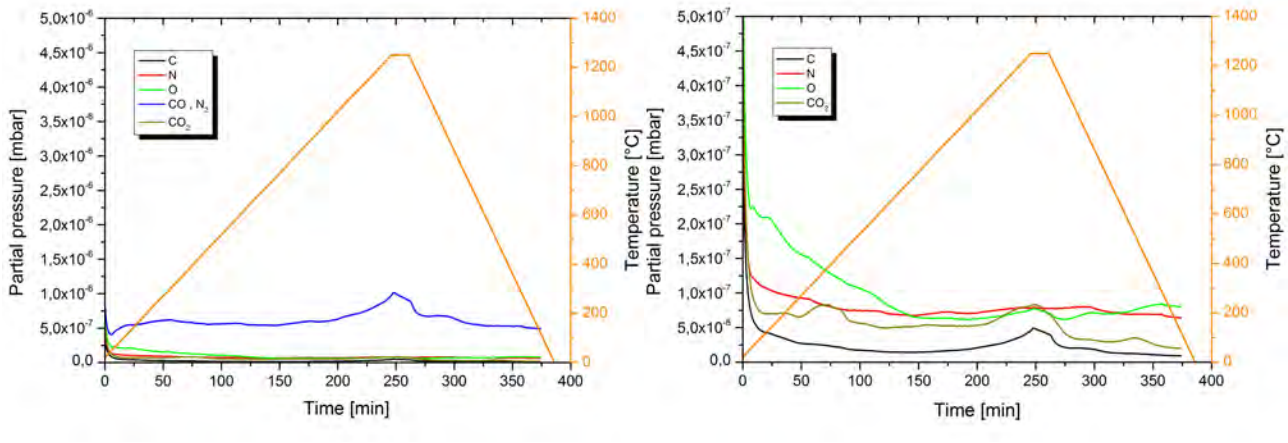

(a) General plot (b) Rescaled

Figure 5. 11: RGA experimental data for PSHTi powder with 1,5% of Carbon added

With the addition of 1,5% of graphite, cannot be observed in Fig. 5. 11 a remarkable change on the general behavior for all the partial pressure with respect to the analysis conducted for PSHTi powder with 0,3% of carbon admixed.
Can be moreover found an increase of the peak's intensity for carbon and mass 28. Taking into account the previous considerations on RGA and not noticing more detection of atomic nitrogen, this indicates that carbon monoxide developed from carbothermal reduction affects more the pressure's signal than molecular nitrogen.

Observations of specimen surface displayed in Fig. 5. 12 indicate no strong connections between particles independently by their size and an evolution of surface's morphology from the case of pure PSHTi powder as more compact layer in relief is visible. The composition in weight of this layer is reported in table 5. 7 and it is based more on Fe, Ti and Cr. The picture maximizing the surface shows also small brighter particle of maximum 0,5μm diameter, whose composition indicates to be formed principally by Titanium (table 5. 7).Other measurements provided in table 5. 8 on this sample were conducted on a sintering neck connecting two particles and on the particle's surface surrounding the neck. As can be seen, iron uptake from particle may be responsible for sintering neck's formation since the surrounding surface's composition shows more amount of oxygen, carbon and titanium.

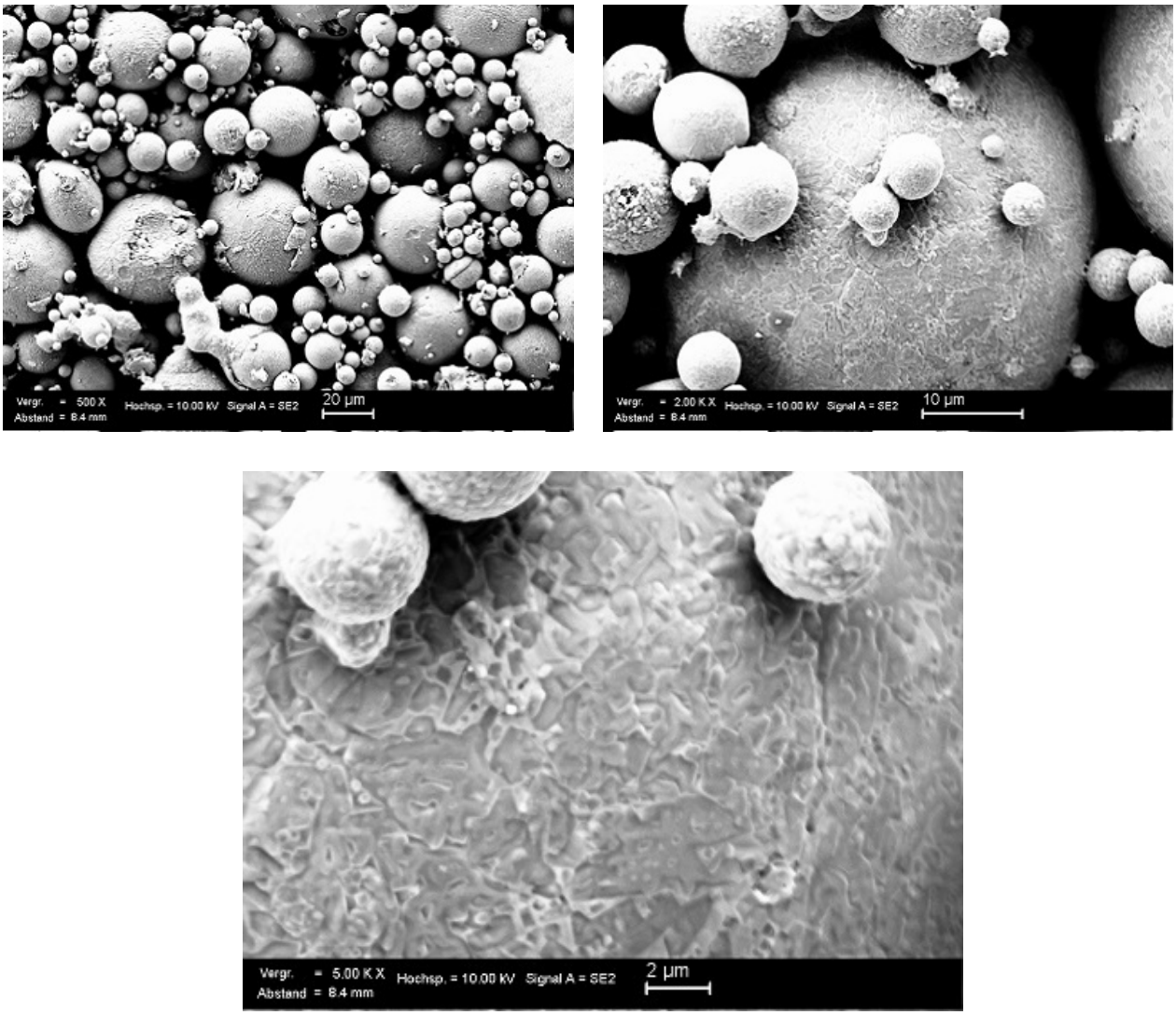

Figure 5. 12: SEM analysis of PSHTi samples surface with 1,5% of graphite

layer			bright particle		
Element	Wt%	At%	Element	Wt%	At%
C K	1.96	7.63	C K	1.15	4.41
O K	1.26	3.66	O K	1.01	2.91
FeL	15.76	13.18	FeL	5.25	4.33
CrK	37.72	33.87	CrK	8.91	7.89
TiK	42.15	41.09	TiK	83.68	80.45
MoL	1.15	0.56	MoL	–	–
Total	100	100	Total	100	100

Table 5. 7: EDX on big particle

neck			surrounding neck		
Element	Wt%	At%	Element	Wt%	At%
C K	2.63	10.17	C K	6.19	20.70
O K	3.78	10.97	O K	4.74	11.92
FeL	73.57	61.20	FeL	52.24	37.58
CrK	10.86	9.70	CrK	7.22	5.58
TiK	7.25	7.03	TiK	28.15	23.61
MoL	1.91	0.93	MoL	1.46	0.61
Total	100	100	Total	100	100

Table 5. 8: EDX on sintering neck

5.2.4 PSHTi with 2% of additional carbon admixed

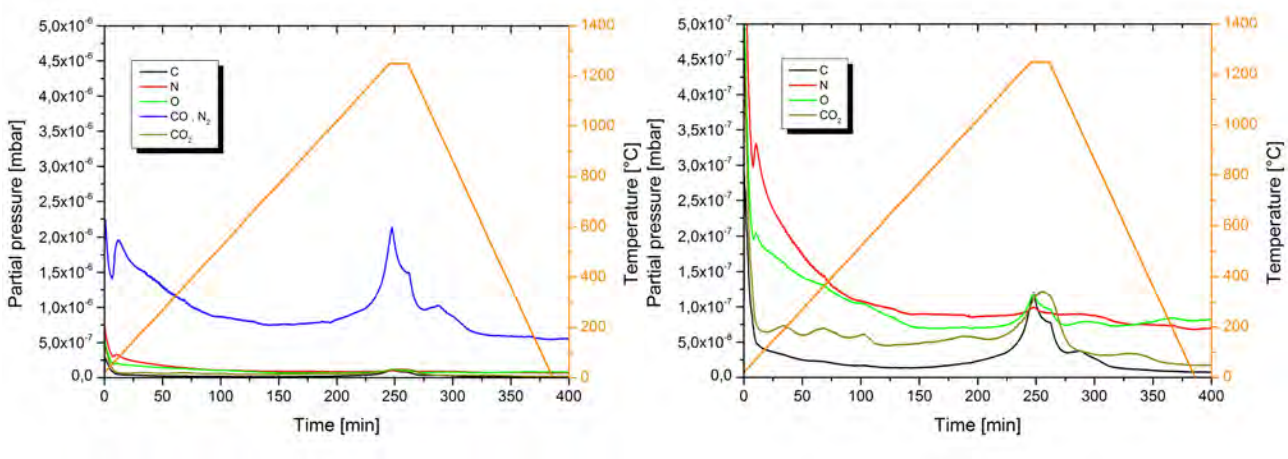

(a) General plot (b) Rescaled

Figure 5.13: RGA experimental data for PSHTi powder with 2% of Carbon added

Fig. 5.13 illustrates the RGA data acquired after the addition of 2% of carbon to PSHTi powder. Regarding masses 12, 16 and 28 an acute characteristic peak is visible once the maximal temperature of 1250celsius is reached. Considering the absence of an evident peak of atomic nitrogen signal, this means that starting at ∼1150 ℃ an evolution of CO from carbothermal reduction is occurring. During the holding time at the maximal temperature a detection of CO_2 is given, in addition to a change of slope characterizing the curves related to carbon, oxygen and carbon monoxide.

With respect to the previous investigations carried out on this powder, an other peak of pressure signal for mass 12 and 28 is present at 1000 ℃ during the cooling process. However, this data is not considered.

5.3 GuiV Powder

5.3.1 GuiV without additional graphite

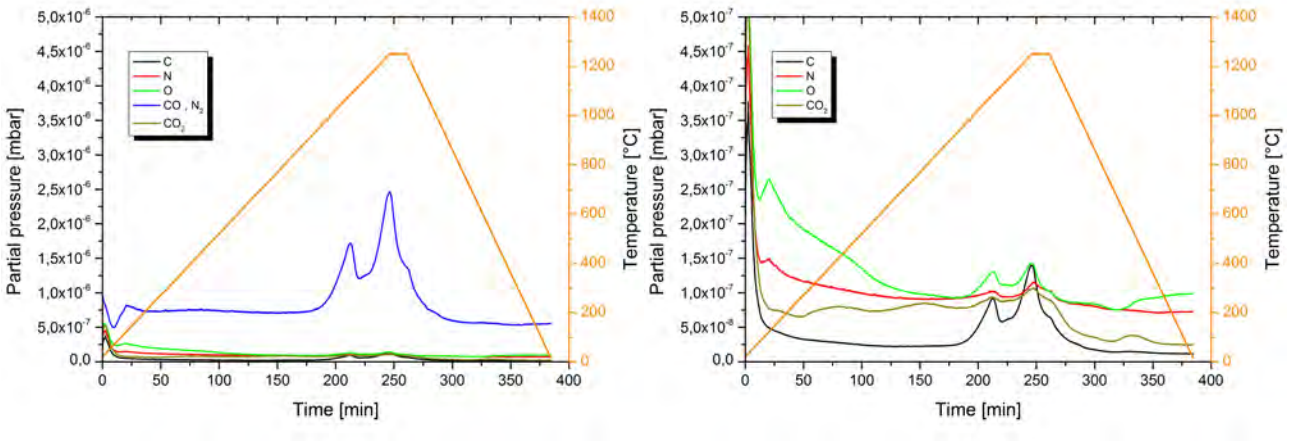

(a) General plot (b) Rescaled

Figure 5.14: RGA experimental data for GuiV powder with 0% of Carbon added

As can be seen in Fig. 5.14 the curves of partial pressure are characterized by two distinct peaks. The first peak has the maximal value of pressure at ∼1100 ℃ and the second peak, more intense, at the temperature of ∼1250 ℃ . Mass 12 and 28 feature a more evident distinction on intensity of the two peaks and again can be noticed that at the beginning of the cooling process there is a change of slope of the curve. In the case of mass 16 the difference of the two peaks is less evident and the average value of pressure is higher with respect to mass 12, 14 and 44. The evolution of atomic nitrogen and carbon dioxide is more pronounced during the holding time at the temperature of 1250 ℃ .

From the analysis conducted on the sample's surface, can be observed the presence of interparticles connections and large round areas of broken surface. Here again, it can be produced by the extraction of the sample from the crucible if a particle's layer bonds with the crucible's inner surface. Increasing the enlargement to 4000x, the Fig.5.15 displays the presence of clean surface and particulates with darker edges. As can be seen in the table 5.9, the EDX measurement on the clean surface shows principally the detection of Fe, Cr and V whereas pointing on the particulates EDX detects also a big percentage quantity of oxygen (table 5.10).

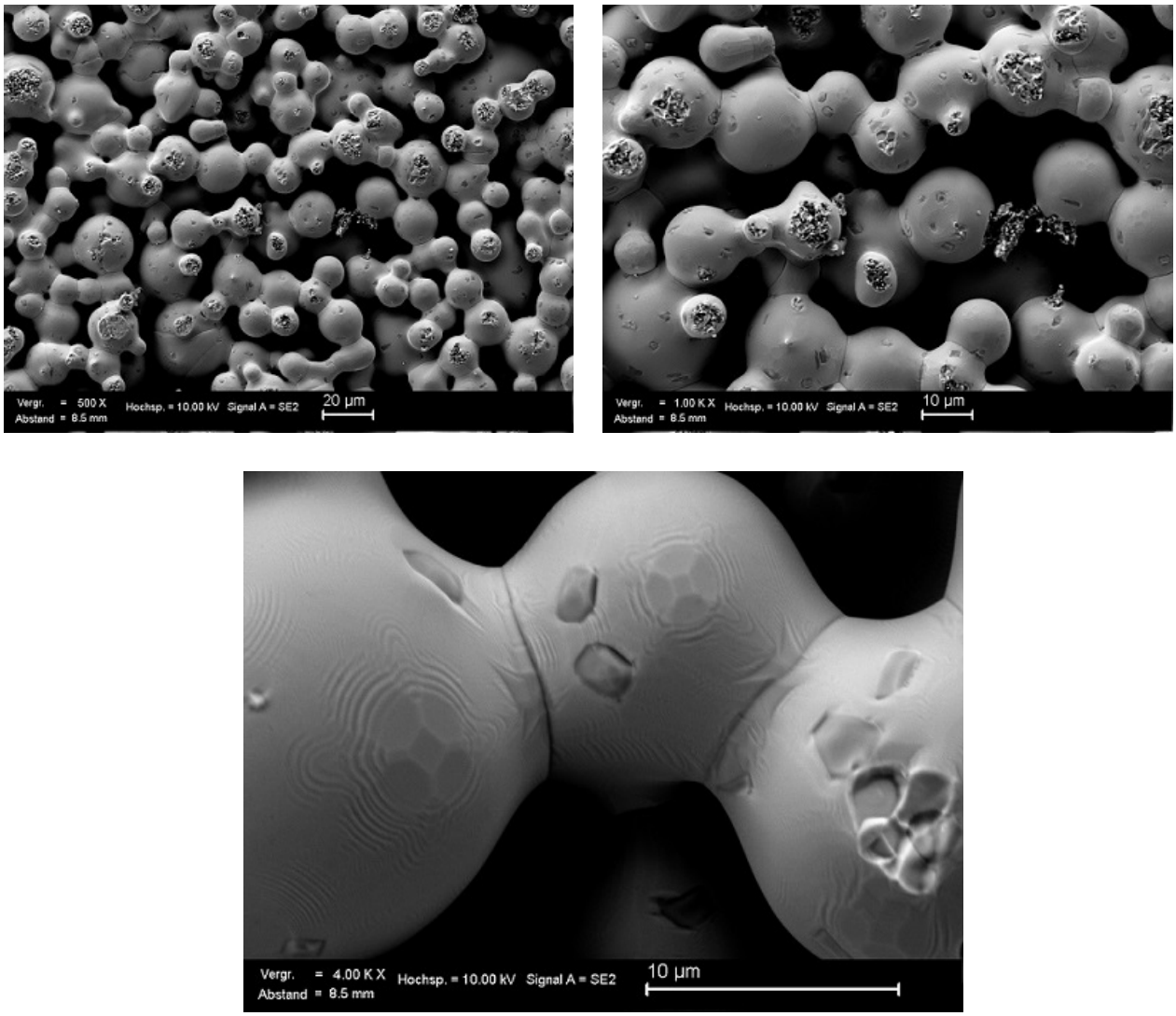

Figure 5. 15: SEM analysis of GuiV samples surface without addition of graphite

Measurement 1		
Element	Wt%	At%
C K	0.84	3.40
O K	3.78	11.51
FeL	62.15	54.18
CrK	21.80	20.41
MoL	0.95	0.48
V K	10.48	10.02
Total	100	100

Table 5. 9: EDX on surface

Measurement 1			Measurement 2		
Element	Wt%	At%	Element	Wt%	At%
C K	5.96	17.11	C K	7.66	19.75
O K	14.02	30.20	O K	18.58	35.96
FeL	16.52	10.20	FeL	3.86	2.14
CrK	5.61	3.72	CrK	3.75	2.23
MoL	1.23	0.44	MoL	1.00	0.32
V K	56.65	38.33	V K	65.14	39.59
Total	100	100	Total	100	100

Table 5. 10: EDX on particulates

In Fig.5. 15 can also be found a characteristic distribution of repeated geometrical imprint not observed in any other powder.

5.3.2 GuiV with 0,3% of additional carbon admixed

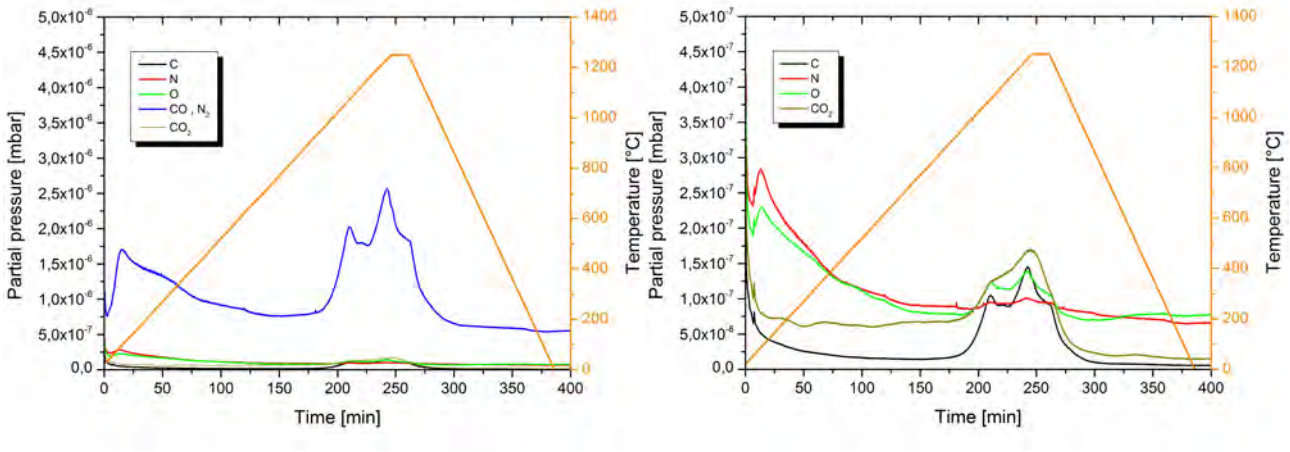

(a) General plot (b) Rescaled

Figure 5.16: RGA experimental data for GuiV powder with 0,3% of Carbon added

Fig. 5.16 displays the same general tendency of all masses found in Fig. 5.15 although 0,3% in weight of carbon has been added. However, can be noticed that the intermediate pressure of mass 28 between the two peaks is higher with the admixing of additional carbon.
Carbon dioxide features an increase on the value of maximal pressure at the temperature of °C corresponding at the principal peak.

5.3.3 GuiV with 1,5% of additional carbon admixed

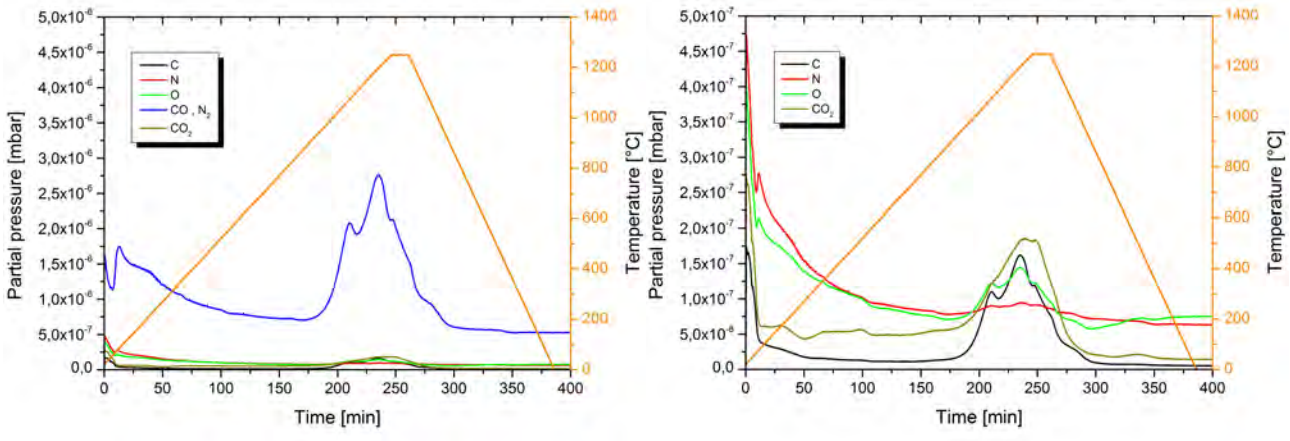

(a) General plot (b) Rescaled

Figure 5.17: RGA experimental data for GuiV powder with 1,5% of Carbon added

The RGA measurement on the GuiV powder with 1,5% of graphite admixed confirms what already observed for the previous experiments on this vanadium pre-alloyed powder steel.
However, can be seen that the secondary and principal peak related to all masses starts now at the temperature of 1100 ℃ whereas in the case of 0% and 0,3% starts at ∼1180 ℃ . The maximal pressure of the principal peak related to mass 12 (C), 16 (O) and 44(CO_2) is found higher adding more carbon in this type of powder.

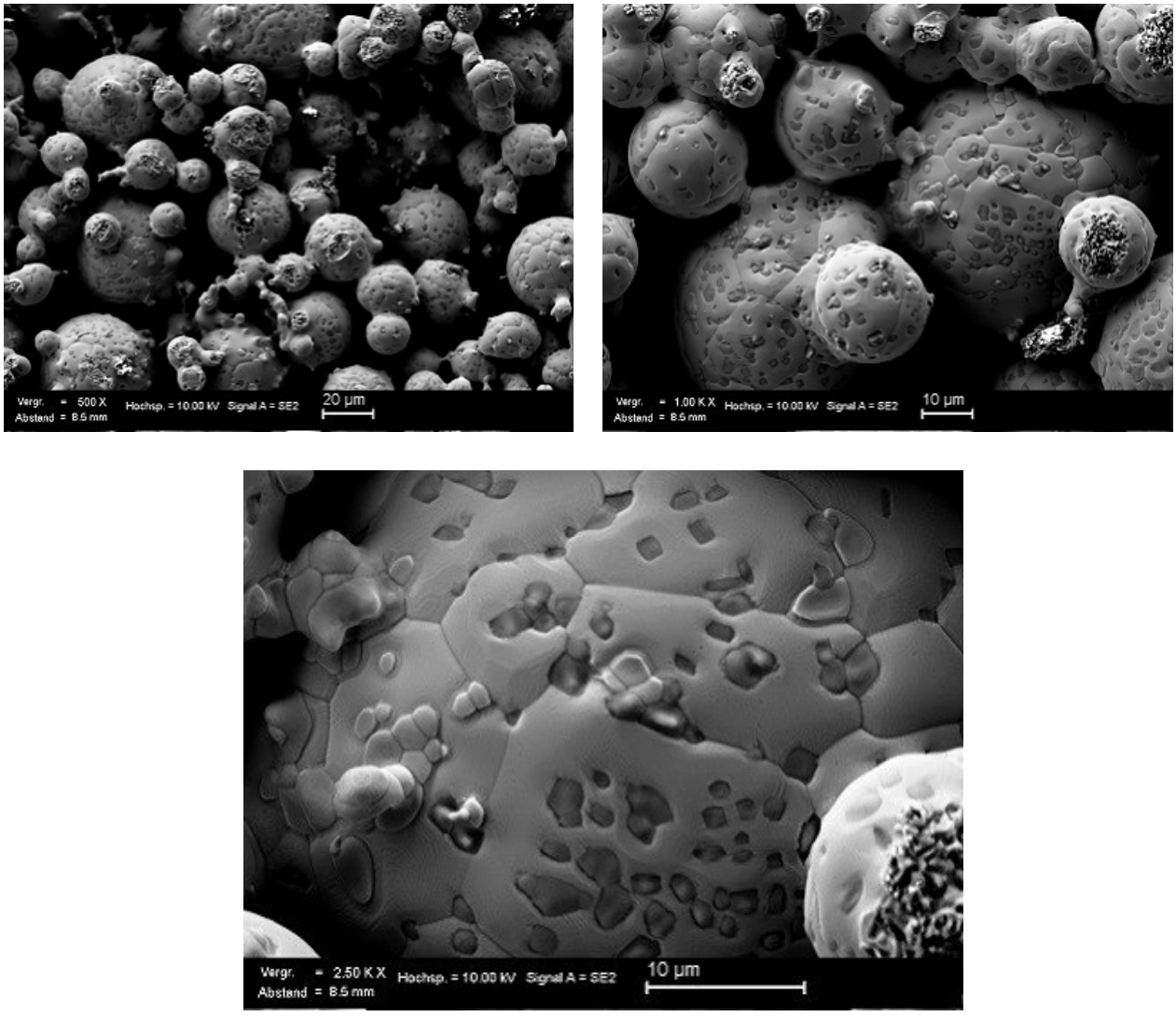

Figure 5. 18: SEM analysis of GuiCr samples surface with 1,5% of graphite

From the observations with SEM and EDX and taking into account the case of GuiV with 0% of carbon admixed, can be seen in Fig. 5. 18 that the surface's morphology is now defined by the presence of plates delimited by boundaries. In these plates are also visible a distribution of darker particulates and isolated bright particles.

As displayed in table 5.11 below, the clean surface of the plates is shown to be more composed by iron (and chromium) whereas darker particulates are formed mostly by vanadium, oxygen and carbon. An EDX analysis made on the brighter small particles features a significant detection of chromium in addition to the elements found in the particulates.

This morphology which seems to be related to the formation of a compact thick layer on the surface may be responsible for the decrease of total quantity of sintering necks with respect to the powder without graphite added.

Measurement 1			Measurement 2		
Element	Wt%	At%	Element	Wt%	At%
C K	1.01	4.07	C K	1.61	6.36
O K	4.00	12.17	O K	3.36	9.94
FeL	73.22	63.75	FeL	43.31	36.71
CrK	16.14	15.09	CrK	35.89	732.67
V K	4.60	4.39	V K	14.93	13.88
MoL	1.02	0.52	MoL	0.90	0.44
Total	100	100	Total	100	100

Table 5.11: EDX on plates surface

bright particles			darker particulates		
Element	Wt%	At%	Element	Wt%	At%
C K	4.65	14.98	C K	5.67	16.27
O K	9.43	22.60	O K	14.41	31.02
FeL	20.99	20.07	FeL	9.86	6.08
CrK	35.88	26.68	CrK	6.27	4.15
V K	19.59	14.07	V K	61.70	41.72
MoL	1.46	0.59	MoL	2.10	0.75
Total	100	100	Total	100	100

Table 5.12: EDX on spots

5.3.4 GuiV with 2% of additional carbon admixed

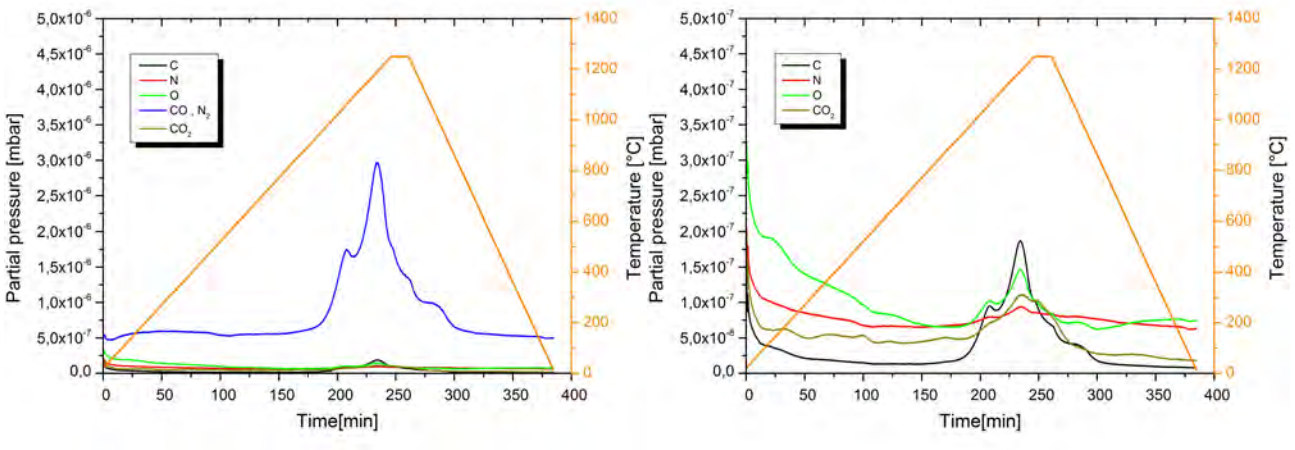

(a) General plot

(b) Rescaled

Figure 5.19: RGA experimental data for GuiV powder with 2% of Carbon added

The addition of 2% of graphite to GuiV powder leads to a similar situation observed with 0,3% and 1,5% of carbon added since the partial pressure of carbon and carbon monoxide exhibits one peak with

a maximal pressure at ~1050 ℃ (50 ℃ less than in the case of pure GuiV) and a more intense second peak with a maximal pressure at 1250 ℃ . According with the contribution of carbon monoxide to the signal of mass 28, the partial pressure of atomic oxygen also shows two peaks at the same temperature but less pronounced on intensities.

The development of carbon dioxide features the same large peak from 1000 ℃ to the beginning of the cooling process.

Chapter 6

Discussion

In this part of the thesis a detailed analysis of the results is presented with references and comparisons with literature data.
In the first three sections the results are discussed considering additional graphs in which the partial pressures of the referring masses are separated and analyzed pointing the attention on the direct influence of carbon addition to them.

6.1 GuiCr

Previous studies conducted on the surface of powders with pre-alloyed chromium indicate that an oxide layer inhomogeneous in thickness covers the powders surface. This oxide layer is formed by a less thermodynamically stable iron oxide layer with a thickness of above 5.5-7nm and particulate compounds (with size above 20-100nm) formed by higher thermodynamically stable oxide of the elements as Cr, Mn and Si [14].
Fig. 6. 1d shows an irregular activity of carbon dioxide not totally consistent with the curve of carbon and carbon monoxide up to 750 ℃. This seems to be in agreement with the Boudouard's equilibrium of graphite oxidation which delineates a major activity of CO_2 below ∼720 ℃.
Since the only reducing agent present is carbon (the constant decrease of water signal confirms that reduction by hydrogen according to equation 2.8 is not taking place), the reduction of the least stable iron oxide layer is expected to occur above ∼800 ℃ [4-5], at which temperature the activity of CO overcomes thermodynamically the one of carbon dioxide and the carbon starts to dissolve into the matrix. Results report a progressive increase of the partial pressure of all masses at 800 ℃ confirming the start of carbothermal reduction of iron oxides.

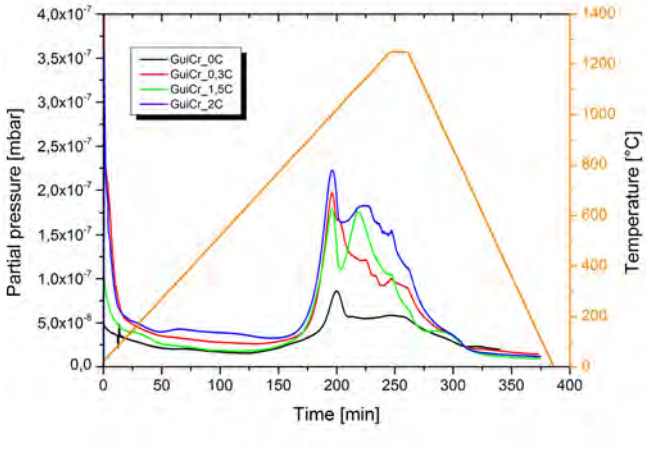

(a) C (mass 12)

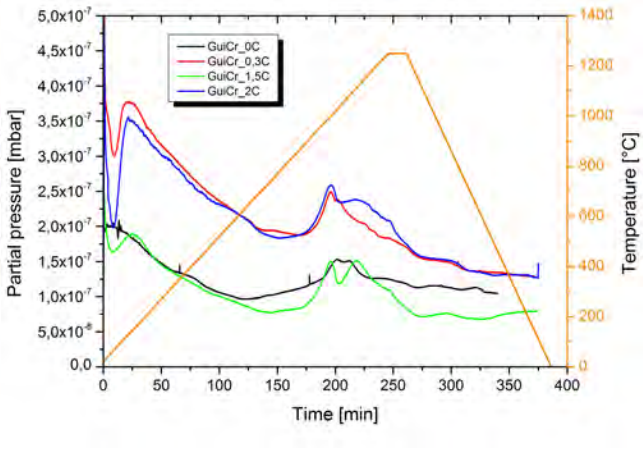

(b) O (mass 16)

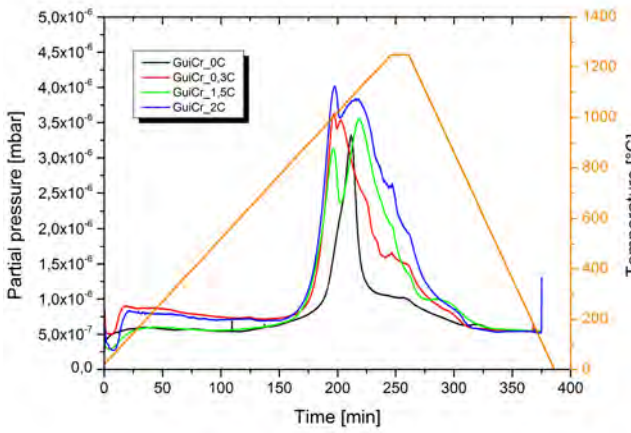

(c) CO, N_2 (mass 28)

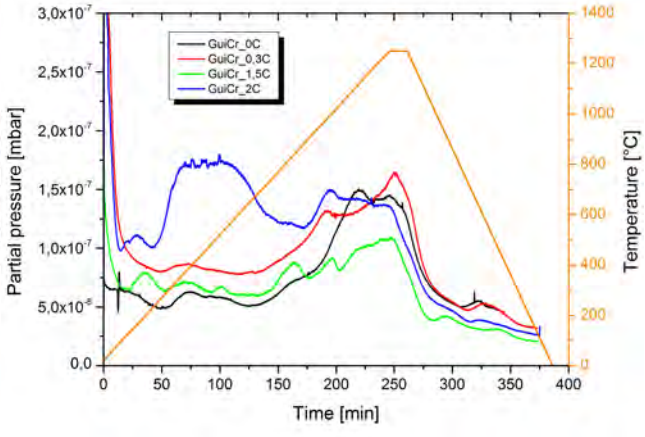

(d) CO_2 (mass 44)

By comparing the slopes of the curves related to CO and CO_2 it can be noticed that, in addition to the strong development of CO from the first direct carbothermal reduction (equation 2.9), also an increase of carbon dioxide pressure is detected. Kinetic model proposed by K. Mondal et al. [7] and based on considerations about thermodynamical stability of iron oxides (especially Hematite: Fe_2O_3, Magnetite: Fe_3O_4 and Wüstite: FeO) promotes the reduction in CO atmosphere to metallic iron at high temperatures through a series of irreversible reaction mechanisms which lead also to the precipitation of iron carbides, shown as follows:

$$Fe_2O_3 + 2CO \rightarrow 2FeO + CO_2 \tag{6.1}$$

$$FeO + CO \rightarrow Fe + CO_2 \tag{6.2}$$

$$3Fe + 2CO \rightarrow Fe_3C + CO_2 \tag{6.3}$$

which can be schematically summarized as:

$$Fe_2O_3 \rightarrow FeO \rightarrow Fe \rightarrow Fe_3C \tag{6.4}$$

In this model Magnetite: Fe_3O_4 is considered a chemical mixture of Hematite and Wüstite thus its role is not considered.

The influence of carbon can be seen in Fig.s 6. 1c and 6. 1a since it shifts the first peak to lower temperature and causes the detection of a secondary peak more intense by admixing more carbon. Starting from ∼1000 ℃, in fact, it has been found that carbothermal reduction of more stable oxides such as Cr-rich oxides takes place. It can be supposed that in the case of GuiCr without addition the smaller amount of carbon in the powder is responsible to the carbothermal reduction which stops as soon as the carbon content is consumed.

Results diverge from the conclusions in previous works [5-12] stated, that more carbon addition is not influencing the reduction behavior, as the carbon content seems to effect remarkably the reduction by varying its concentration. However, it has to be considered that in this case the powders under investigation are much higher alloyed in Chromium, which leads to a major complexity and a bigger amount of stable oxides to be reduced.

As mentioned above, from ∼1080 ℃ the profile of the partial pressure of carbon monoxide is correlated to the amount of carbon added, reasonable derived by the reduction of iron oxides from the inner core of the powder particles and the simultaneous reduction of oxides formed by chromium (and less part by manganese).

Specific calculations of reduction of Cr_2O_3 by graphite were advanced by E. Hryha et al. [6] which indicate that at the usual sintering temperature of 1120 ℃ the following reaction:

$$\frac{1}{3}Cr_2O_3 + C \rightleftharpoons \frac{2}{3}Cr + CO \tag{6.5}$$

proceeds spontaneously if p(CO) is less than 0,195bar. This is condition easily reached in high vacuum and confirmed by the peak observed for masses 12 and 28 at that temperature after addition of 1,5% and 2% of graphite.

However, it can be noticed in the Fig. 6. 1d that the carbon content does not show a specific influence on the evolution of carbon dioxide as observed for carbon monoxide. This may be explained since high temperatures enhance direct carbothermal reduction of oxides instead of the indirect one, independently by the carbon content.

From observations with SEM there cannot be seen the same quantity of bright particles rich on oxygen and elements forming stable oxides such chromium and aluminium for powder admixed with graphite, showing furthermore a slightly improvement of interparticle connection.

It can be noticed in the Fig. 5. 5 a big amount of dark particulates mostly formed by carbon, probable residual of graphite not dissolved, and the characteristic grooves rich on iron and chromium related to the evaporation process.

6.2 PSHTi

In the case of PSHTi powder, the consequences of the graphite addition are summarized by the following graphs. Increasing the weight percentage of carbon, the curves describing the partial pressure

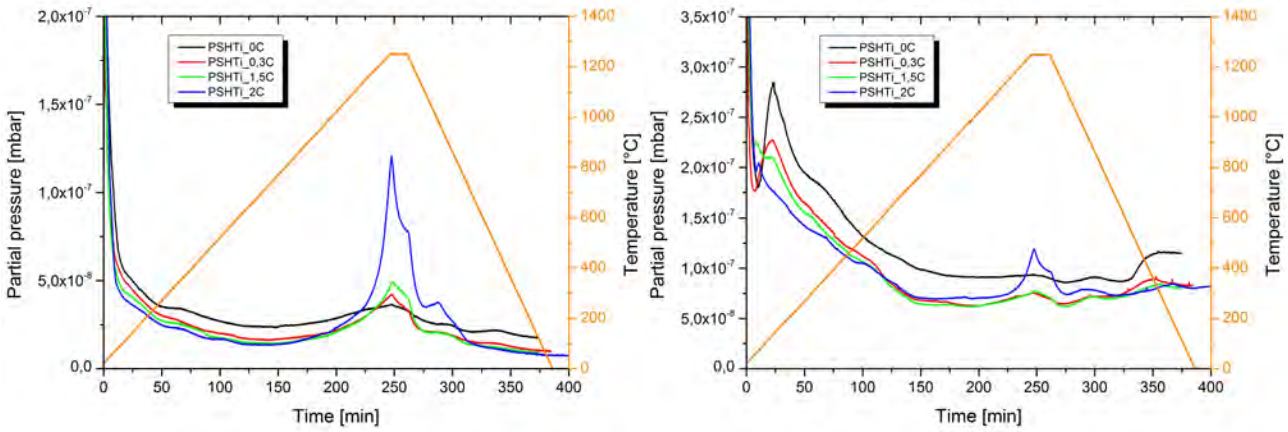

(a) C (mass 12)

(b) O (mass 16)

(c) CO, N_2 (mass 28)

(d) CO_2 (mass 44)

of mass 28 and mass 12 (less for atomic oxygen) show an identical profile characterized by an increase of the peak's intensity after increasing the carbon content. This indicates the same existing correlation between the graphite added and the carbothermal reduction taking place observed for GuiCr powder. The beginning of the carbothermal reduction does not exhibit a strong dependency with the graphite

content since all the referring peaks of carbon and carbon monoxide are shown to start approximately at the temperature of 1000 ℃. The data acquired by experiments conducted on the powder without the addition of carbon do not display evident evolution of carbon, oxygen and carbon monoxide. One explanation could be that titanium has an higher affinity for oxygen than iron and chromium and this means that oxygen from the exposition to air tends to form more titanium-based oxides which cannot be reduced at that temperature (Fig. 2. 6). However, the exclusive presence of titanium oxides is excluded as well due to carbothermal reduction clearly occurring by adding graphite and involving iron and chromium oxides.

Therefore, It may be suggested that in the case of PSHTi without graphite, with respect to pure GuiCr powder which shows a peak of carbon monoxide, the carbon present in alloy, although in lower concentration, can be responsible of iron and chromium oxides reduction but with the immediate reaction of carbon monoxide with high reactive titanium forming precipitation of carbide or stable titanium oxides, contributing for steel carburization via gaseous mass transfer of carbon(2.2). This can explain the presence of carbon on the surface detected with SEM and EDX and the presence of a carbon dioxide's evolution.

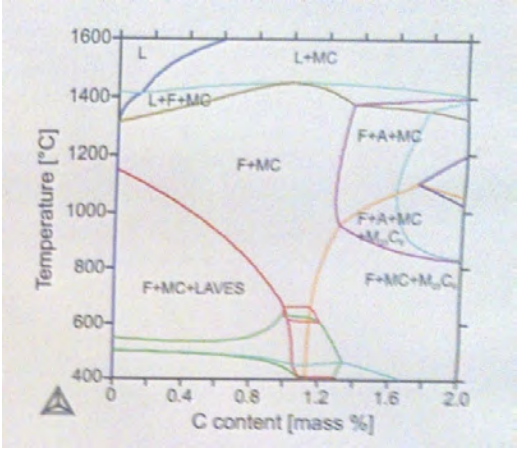

Figure 6. 3: Phase diagram Fe-15Cr-5Ti

Previous thermodynamic calculations conducted by S. Huth and H. Schaar on Fe-15Cr-5Ti carbon-free steel shown in Fi. 6. 3 and the Fe-Ti phase diagram indicate at the temperature of ∼1100 ℃ the complete dissolution of Laves phase formed by the intermetallic compound Fe_2Ti into the ferric lattice.

With the addition of 1,5% and 2% of graphite, the carbon amount may be sufficient for a deep diffusion into the particle reaching and reducing more iron and chromium oxides, increasing CO evolution. However, the partial pressure of carbon dioxide is not showing evident difference adding 2% of graphite and this seems to confirm the supposition above since titanium dissolved in lattice is the limiting agent in the reaction with CO developing carbon dioxide.

As already discussed for GuiCr, the decrease of atomic oxygen's signal during the heating process may be related to the similar profile assumed by the partial pressure of H_2O, developed by the decomposition of hydrate metallic compounds, oxyhydroxides or water's molecules adsorbed by the particles surface. Data acquired from analysis conducted on the surface does not give sufficient information to predict the exact type of species present on the surface. From observations with SEM and EDX it can

be seen that with increasing the amount of graphite added the carbon content detected on the surface has not increased, as it was expected. Considering that the partial pressure of CO is higher adding more graphite, it can be supposed that higher pressure of CO promotes oxides reduction instead of carbon deposition. However, this hypothesis is not actually confirmed by previous investigations in the same contest.

6.3 GuiV

Regarding the powder with an important amount of vanadium alloyed, the results presented in the previous chapter and in the Fig.s below feature some differences and similar behaviors with respect to GuiCr and PSHTi. Fig.s related to the partial pressure of masses 12 and 28 show an identical profile

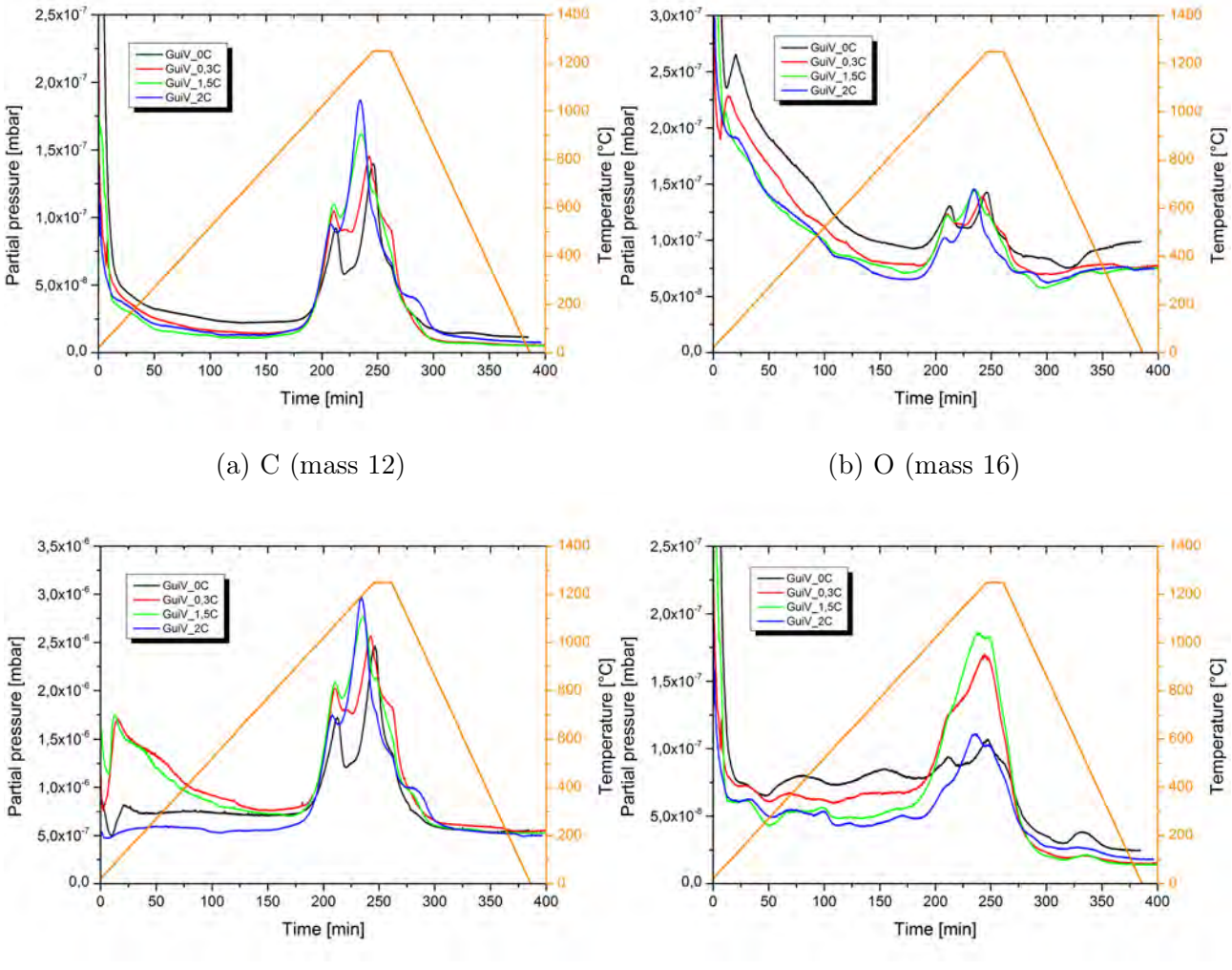

(a) C (mass 12)

(b) O (mass 16)

(c) CO, N_2 (mass 28)

(d) CO_2 (mass 44)

with the obvious difference of the magnitude of the values. In both cases the addition of graphite leads to an increase of the principal secondary peak's intensity and the shift of the maximal pressure to lower temperature values (from 1250 ℃ for pure GuiV to 1190 ℃ with 2% of carbon added); whereas the first and less pronounced peak does not show an evident correlation with the carbon addition. However, the more graphite is added, the higher is the partial pressure of C and CO is detected from 1100 ℃. This indicates again a stronger interaction of carbon with the powder if added in higher percentages. The first peak features the maximal value of pressure at the temperature of ∼1100 °C, the same range is registered in the case of the GuiCr powder without carbon added. It is therefore possible that in this range of temperature the carbothermal reduction of stable Cr-rich oxides occurs, in the way already discussed above and in accordance with literature values [4-11]. The secondary and principal peak is clearly related to the evolution of carbon monoxide from the carbothermal reduction of more stable oxides such vanadium oxides. Fig. 6. 5 beside shows the oxygen partial pressure in equilibrium with vanadium oxides, especially V_2O_5, V_2O_4, V_2O_3 and VO. The reactions which increase the oxidation state of vanadium from V to II (respectively), with evolution of oxygen, are strongly endothermic with positive free enthalpies up to 2000K.

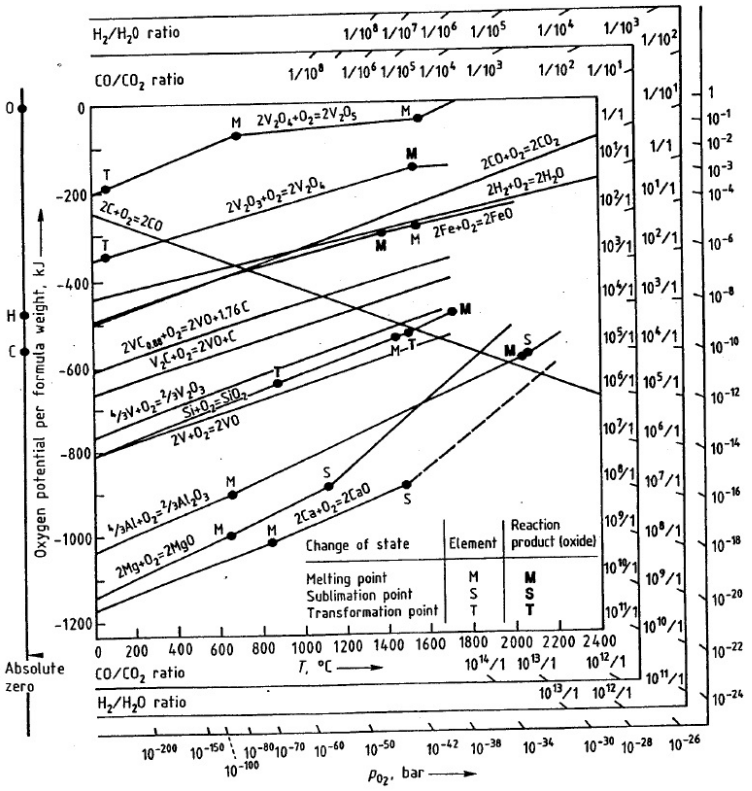

Figure 6. 5: Oxygen potential of oxides of vanadium as a function of temperature

However, in presence of reducing gases such as CO (or H_2) higher oxides are directly reduced to V_2O_3 with evolution of carbon dioxide. Previous studies report that the reduction of V_2O_3 to VO by oxydation of CO to CO_2 does not go to completion whereas the reduction by carbon almost does:

$$V_2O_3 + C \rightarrow 2VO + CO \tag{6.6}$$

However, the reaction of VO with carbon gives initially vanadium carbide according with:

$$VO + 1.88C \rightleftharpoons VC_{0.88} + CO \tag{6.7}$$

and only the subsequent reaction of oxide with carbide can eventually reduce to metal vanadium.

$$VO + 1.14VC_{0.88} \rightleftharpoons 2.14V + CO \tag{6.8}$$

However, it has been known that VO and C are soluble in vanadium at high temperature, not promoting the carbothermal reduction to pure vanadium metal [9].
From the observations of the specimen's surfaces without and with the addition of 1,5% of graphite and taking into account the general behavior shown in the graphs above, it can be noticed that the amount of carbon pre-alloyed present in the GuiV powder is sufficient for reduction of stable oxides formed by Chromium and Vanadium, since the mass loss of carbon and carbon monoxide display the two characteristic peaks at different temperature ranges, respectively. On the other hand, a comparison of Fig.s 5. 15 and 5. 18 shows and confirms that the evolution of CO is not only derived by the reduction of oxides following e.g. the reaction 6.6 but in both cases gaseous CO is developed by reactions forming vanadium carbides, precipitated and observed as dark spots on the surface. Furthermore, the detection of bigger amount of carbon, oxygen and vanadium on the dark spots with respect to the clean surface more rich in iron and chromium suggests that vanadium oxides might also act as preferable sites for carbides precipitation, instead reaching their total reduction.
Adding 1,5% of graphite does not lead to an improvement of oxides reduction but moreover it deteriorates evidently the formation process of interparticle connections and promotes the precipitation of dark spots rich on carbon and oxygen.

6.4 Comparison

An addition of graphite to the GuiCr leads to a shift of the maximal pressure of the first peak related to the carbothermal reduction (C,CO) of the chromium oxides to lower temperature, to an increase of the intensity of the first peak proportionally to the percentages of graphite admixed and to a detection of a secondary peak which intensity also depends on the carbon added. This phenomena occurs also partially for GuiV whereas the first peak (with the maximum slightly at higher temperatures) does not show a strong dependency to the carbon content. This could be explained considering that the higher affinity of vanadium for oxygen causes a primary formation of more stable oxides rich on V instead of Cr. This means that the low carbon amount in unadmixed GuiV powder is sufficient for the reduction of Cr-rich oxides with respect to the bigger quantity of chromium oxides in GuiCr. The reduction of oxides inside the powder particles and oxides formed by vanadium requires more carbon with an observed shift of the maximum of the second peak to lower temperatures. The case of PSHTi reports

the same reduction of the chromium oxides starting from 1000 °C (visible from the signal of CO_2) although a more evident increase of the CO evolution is shown at 1200 °C and adding 2% graphite. Furthermore, for this powder the peaks are limited by the end of the heating process, suggesting that the presence of titanium might affect the reduction by requiring higher temperatures.

From the comparison of the SEM and EDX observations the addition of 1,5% graphite has been shown to improve the connections between particles only in the case of GuiCr, whereas for GuiV the powder features a higher quantity of dark spots and the formation of a compact layer seems to obstacle the formation of sintering necks. Measurements regarding PSHTi powder also seem to confirm the same tendency of promotion of a compact layer instead of sintering interconnections.

Chapter 7

Conclusions and future work

The usage of these powders admixed with graphite is meant to provide the PM parts with the high standard properties required nowadays for mechanical components, taking into account the flexibility and the economic convenience of the industrial process.
The diffusion alloying method currently under investigation is offering a different approach to the process leading to the necessary reduction of oxides and the carburization of the powder steel. However, the presence of elements with high affinity to both oxygen and carbon makes of remarkable importance the complete understanding of the mechanism which rules first the reduction of oxides deteriorating the mechanical properties and subsequently the formation of carbides increasing the properties itself.
The conclusions can be summarized as follow:

- The effect of graphite addition depends on the type of powder although for all powders it did lead to an increase of the carbon monoxide detection by carbothermal reduction of oxides.
- As seen especially in GuiCr powder, it seemed to affect the temperature start of the chromium oxides reduction and promote the reduction of oxides from the inner core of the particles by diffusion of carbon. Graphite slightly improved the sintering process.
- the effect on PSHTi is still unclear. On one hand it enhanced the development of CO but not the formation of sintering necks. The SEM analysis showed the creation of a compact layer. An more detailed X-ray analysis would have indicated the composition of this layer.
- In the case of GuiV an higher concentration of graphite seemed to inhibit the formation of inter-particle connections. A better understanding of the correlation between oxide reduction and carbide formation is needed.

The thermodynamical complexity of the reactions and the quantity of variables involved in both processes enhance drastically the difficulty level of the challenge and additional experiments are needed. It would be especially interesting to investigate the influence of the graphite particle size, the effect

of different mixing modalities, with the intention to obtain a higher homogeneity of the mixture, and the effect of a pressure induced. Additional tests as XRD and XPS would have served for a better individuation of the chemical species on the surface, providing information about the presence of more complex ternary oxides instead of binary ones or inter-metallic phases.

Bibliography

[1] S. Huth, N. Krasokha, W. Theisen, Development of wear and corrosion resistant cold-work tool steels produced by diffusion alloying, Wear, Volume 267, Issues 14, 15 June 2009, Pages 449-457,

[2] S. Huth, W. Theisen, Diffusion alloying : a new manufacturing method for PM tool steels, Powder Metallurgy, Volume 52, Issue 2, 2009, Pages 90-93,

[3] E. Hryha, et al, Surface composition of the steel powders pre-alloyed with manganese, Applied surface science, Volume 256, Issue 12, 2010, Pages 3946 3961,

[4] S. Huth, K. Zumsande, L. Mujica, N. Krasokha, W. Theisen, Oxide Reduction During Carburization Nb-Rich Tool Steel Powders for Diffusion Alloying, Powder Metallurgy, Volume 55, Issue 5, 2012, Pages 323-328,

[5] H. Danninger, C. Gierl, S. Kremel, G. Leitner, K. Jaenicke-Roessler, Degassing and deoxidation processes during sintering of unalloyed and alloyed PM steel, Powder Metallurgy Progress, Volume 2, Issue 3, 2002, Pages 125-140,

[6] E. Hryha, L. ajková, E. Dudrová, Study of reduction/oxidation processes in Cr-Mo prealloyed steels during sintering by continuous atmosphere monitoring, Powder Metallurgy Progress, Volume 7, Issue 4, 2007, Pages 181-197,

[7] K. Mondal, H. Lorethova, E. Hippo, T. Wiltowski, S.B. Lalvani, Reduction of iron oxide in carbon monoxide atmosphere: reaction controlled kinetics, Fuel Processing Technology, Volume 86, Issue 1, 15 November 2004, Pages 33-47,

[8] W.K. Jozwiak, E. Kaczmarek, T.P. Maniecki, W. Ignaczak, W. Maniukiewicz, Reduction behavior of iron oxides in hydrogen and carbon monoxide atmospheres, Applied Catalysis A: General, Volume 326, Issue 1, 30 June 2007, Pages 17-27,

[9] G. Bauer, V. Güther, H. Hess, A. Otto, O. Roidl, H. Roller, and S. Sattelberger, Vanadium and Vanadium Compounds. Ullmann's Encyclopedia of Industrial Chemistry, Volume A27, Issue 2000, Pages 367-386

[10] M. Nabeel, Diffusion of Elemental Additives during Sintering, KTH, Materials Science and Engineering, 2012,

[11] Boris V Lvov, Mechanism of carbothermal reduction of iron, cobalt, nickel and copper oxides, Thermochimica Acta, Volume 360, Issue 2, 28 September 2000, Pages 109-120,

[12] D. Chasoglou, E. Hryha, L. Nyborg, Effect of sintering atmosphere on the transformation of surface oxides during the sintering of chromium alloyed steel, Powder Metallurgy Progress, Volume 9, Issue 3, 2009, Pages 141-155,

[13] M. Goeckner, Lab 7: Residual Gas Analyzers, The University of Texas, 2002,

[14] O. Bergman, Key Aspects of Sintering Powder Metallurgy Steel Prealloyed with Chromium and Manganese, CTH, Department of Materials and Manufacturing Technology, 2011,

[15] G. Dowson, Introduction to Powder Metallurgy, EMPA, [2008]1992,

[16] A. Weddeling, Surface Analysis of Austenitic Fe-18Cr-19Mn-C-N Powder, CTH, Department of Materials and Manufacturing Technology, 2011,

[17] The Metal Powder Industries Federation (MPIF), Web Site, College Road East,

[18] P.C. Angelo, R. Subramanian, Powder Metallurgy: Science, Technology and Applications, PHI Learning, 2008,

[19] G. I. Goldstein, D. E. Newbury, P. Echlin, D. C. Joy, C. Fiori, E. Lifshin, Scanning electron microscopy and x-ray microanalysis. New York: Plenum Press, 1981

[20] B. Cheney, Introduction to Scanning Electron Microscopy, SJSU, Materials Engineering Department,

[21] E. Hryha, E. Dudrova, L. Nyborg, On-line control of processing atmospheres for proper sintering of oxidation-sensitive PM steels, Journal of Materials Processing Technology, Volume 212, Issue 4, 2012, Pages 977-987,

Riassunto

Nella produzione di componentistica meccanica e di utensili da taglio, la metallurgia delle polveri ha assunto una notevole importanza negli ultimi due secoli a causa della flessibilità ed economicità del processo, consentendo la produzione di componenti con forma complessa e specifiche proprietà. Nel caso di utensili da taglio, fondamentali sono le proprietà di resistenza a corrosione ed usura. La prima può essere ottenuta con l'alligazione di cromo e la seconda con la dispersione di una fase di carburi in matrice metallica. A causa dell'elevata affinità del cromo sia per l'ossigeno che per il carbonio per la formazione di carburi e per preservare la necessaria quantità di cromo per la resistenza a corrosione, si può, contestualmente all'aumento del tenore di carbonio per favorire la precipitazione di carburi, aumentare il quantitativo totale di cromo oppure aggiungere in lega elementi formatori di carburi con più elevata affinità per il carbonio del cromo, come vanadio, titanio o niobio. Non è tuttavia tecnologicamente possibile produrre polveri di acciaio tramite atomizzazione a gas partendo da un fuso contenente i suddetti elementi ed il carbonio a causa della primaria ed incontrollata precipitazione di carburi che possono otturare l'orifizio dell'unità di atomizzazione. In questo contesto, *Diffusion Alloying Method* si è imposto come una promettente tecnica di produzione di utensili a freddo carburizzati e prevede la produzione di polveri di acciaio con basso contenuto di carbonio ma altamente legato con elementi formatori di carburi, e la successiva aggiunta di grafite prima del processo di sinterizzazione. La grafite infatti agisce come lubrificante, aumenta la durezza dell'utensile e favorisce la riduzione degli ossidi superficiali delle polveri. La riduzione degli ossidi è di fondamentale importanza in quanto in sede di sinterizzazione e nel processo di alligazione per diffusione costituiscono una barriera, deteriorando così le proprietà meccaniche finali del componente sinterizzato. Questa tesi si poneva l'obiettivo di contribuire alla caratterizzazione del processo di riduzione degli ossidi in polveri d'acciaio miscelate con diverse quantità di grafite, tramite il monitoraggio della fase gas sviluppata nel processo di sinterizzazione sottovuoto.
La parte sperimentale consisteva nella preparazione dei crogioli di allumina con trattamento

ad ultrasuoni in soluzione di etanolo, asciugatura ed eliminazione di eventuali residui tramite cottura sottovuoto a 1300 °C per 3h. La giusta quantità di grafite in rapporti ponderali prestabiliti (0,3%, 1,5% e 2%) è stata manualmente aggiunta in laboratorio in atmosfera controllata di azoto; a cui è seguito un processo di mescolamento di 30 minuti. Il processo di sinterizzazione è stato eseguito in condizione di elevato vuoto dinamico ($2 \cdot 10^{-5}$ mbar), con un riscaldamento di 5K/min ed un massima temperatura di 1250 °C mantenuta per 15 minuti. La fornace e la pompa a vuoto turbomolecolare erano collegati ad uno spettrometro di massa (RGA) che monitorava la pressione parziale dei gas sviluppati nei processi riduttivi degli ossidi alle varie temperature. Le polveri di acciaio sinterizzate senza grafite e con 1,5% di grafite sono state poi analizzate al microscopio a scansione elettronica con dispersione a raggi X, per verificare l'effetto della grafite nel processo di formazione di colli di giunzione e l'eventuale composizione chimica di particelle superficiali quali potessero essere ossidi non ridotti o carburi precipitati.

Le tre polveri utilizzate presentano diversa composizione chimica. GuiCr è una polvere d'acciaio al cromo (15,57%) e legato con diversi elementi: 0,16%C , 0,52%Ni , 1,02%Si, 0,52%Mn, 0,6%Mo e 0,04%Al.

PSHTi presenta un tenore di carbonio del 0,09%, un contenuto di cromo e di molibdeno rispettivamente del 13,81% e 1,1% ed è legato con 5,09% di titanio.

La polvere d'acciaio GuiV è invece composta da: 0,37%C, 17,08%Cr, 0,66%Mo e 7,02%V.

Dalle misurazioni effettuate sulla polvere GuiCr senza l'aggiunta di grafite, si può notare come la pressione parziale della massa 28uma, corrispondente al monossido di carbonio (ed azoto molecolare(, presenti un aumento di intensità a partire da ∼800 °C , temperatura di inizio riduzione degli ossidi di ferro in presenza di carbonio come agente riducente. A temperature superiori a 720 °C infatti, la grafite si dissolve nell'acciaio e si entra nel campo di stabilità del monossido di carbonio. A partire da 970 °C è evidente un notevole aumento della pressione parziale di CO con un picco il cui massimo è stato registrato a 1080 °C . Precedenti studi confermano che a temperature superiori a ∼1000 °C ha luogo la riduzione dei più stabili ossidi di cromo superficiali con riduzione diretta ed indiretta. Aggiungendo grafite in percentuali più elevate, si può notare come questa provochi un anticipazione del principale picco a temperature inferiori e la creazione di un picco secondario con base più larga. Questo può essere spiegato considerando che un aumento del contenuto di carbonio provoca una più rapida riduzione

degli ossidi superficiali ed una più profonda diffusione del carbonio stesso nelle particelle, raggiungendo e riducendo gli ossidi interni. Dalla caratterizzazione della superficie dei campioni effettuata al microscopio a scansione elettronica, è possibile osservare come l'aggiunta di 1,5% di grafite ha portato ad un leggero miglioramento dell'interconnessione tra particelle ed alla riduzione di particelle ed agglomerati superficiali trovati nel caso di polvere senza grafite, caratterizzati da un elevato contenuto di ossigeno ed elementi fortemente formatori di ossidi come Mn e Cr.

Dalle analisi eseguite sulla polvere PSHTi, acciaio legato con una consistente quantità di titanio, è possibile fare diverse considerazioni. La misurazione dei gas residui nel caso della sola polvere rivela l'assenza di un picco di monossido di carbonio, come rilevato per la polvere GuiCr, ma la contemporanea presenza di un picco della pressione parziale della massa 44uma, corrispondente all'anidride carbonica, a partire dalla temperatura di 1050 °C . Aggiungendo 0,3% e 1,5% di grafite si può notare un lieve aumento della pressione parziale di CO con un picco il cui apice corrisponde alla fine del processo di riscaldamento alla temperatura di 1250 °C . Solo a seguito dell'aggiunta del 2% si nota un considerevole aumento della pressione di monossido di carbonio, nonostante non sia visibile la stessa dipendenza dal contenuto di grafite nel caso del segnale corrispondente all'anidride carbonica. La fine inoltre del picco corrisponde all'inizio del processo di raffreddamento, con un cambiamento netto della pendenza delle curve.

Nonostante il contenuto di carbonio sia inferiore rispetto a GuiCr e considerando l'elevata stabilità degli ossidi di titanio che richiedono più elevate temperature per la riduzione, lo sviluppo di anidride carbonica sembra comunque confermare la riduzione di ossidi superficiali, verosimilmente del ferro e del cromo. Tuttavia un mancato sviluppo di monossido di carbonio, considerando le precedenti analisi e la maggiore stabilità del monossido di carbonio alle elevate temperature, potrebbe essere spiegato dall'evoluzione alle elevate temperature della struttura stessa dell'acciaio. Precedenti simulazioni termodinamiche mostrano infatti alla temperatura di $\sim$1100 °C la completa dissoluzione della fase intermetallica di Lavè Fe_2Ti nella matrice ferritica, permettendo eventualmente all'altamente reattivo titanio di reagire superficialmente con il monossido di carbonio sviluppato consumandolo e producendo anidride carbonica con la precipitazione di carburo di titanio. All'aumentare del contenuto di grafite aggiunta, l'evoluzione di monossido di carbonio risulta più marcata in quanto maggior carbonio reagisce riducendo gli ossidi di cromo e la reazione col titanio è altresì limitata dalla quantità di titanio

dissolto superficialmente nel reticolo ferritico. Non sono stati tuttavia trovati recenti riscontri a dimostrazione della precedente supposizione, rendendo necessarie ulteriori analisi e simulazioni della cinetica di reazione. Dalle analisi al microscopio a scansione elettronica non sono stati riscontrati, successivamente all'aggiunta di grafite, miglioramenti sulla giunzione della particelle a seguito del processo di sinterizzazione e si può notare la formazione di uno strato compatto sulla superficie stessa. Non è stato tuttavia possibile determinare la natura chimica di tale strato a causa della mancata disponibilità di ulteriore caratterizzazione tramite XRD. Nel caso della polvere GuiV, che presenta una consistente concentrazione di vanadio, è stato osservato come le pressioni parziali di CO e C (che confermano il predominante contributo del monossido di carbonio al segnale di massa 28uma) presentano un primo picco con il massimo alla temperatura di 1080 ℃ ed un secondo picco di maggiore intensità a 1200 ℃ . Aggiungendo grafite in quantità sempre maggiori si può notare come il primo picco non subisce evidenti modificazioni, ed un più marcato effetto viene registrato per il secondo, che viene anticipato a temperature inferiori con un contemporaneo aumento dell'intensità del picco stesso.

Questo può essere spiegato considerando la più elevata affinità del vanadio per l'ossigeno e la conseguente maggiore quantità dei suoi ossidi, rispetto a quelli di cromo. Il tenore di carbonio della polvere risulta quindi sufficiente per la riduzione degli ossidi di cromo alla temperatura di ∼1080 ℃ e l'aggiunta del carbonio produce un effetto solo sulla riduzione dei più stabili ossidi di vanadio e sulla riduzione degli ossidi interni, così come è stato verificato nei precedenti studi effettuati sulle altre due tipologie di polveri.

Dall'analisi al microscopio si può notare però come l'aggiunta di 1,5% di grafite peggiori la formazione di colli di giunzioni tra le particelle ed il processo di sinterizzazione, nonostante sia evidente una maggiore riduzione di ossidi metallici, e causi la formazione di particelle di contrasto più scuro, ricche anche di carbonio. Questo può essere spiegato dalla particolare cinetica di riduzione degli ossidi di vanadio che, in presenza di carbonio come agente riducente, si riduce dal suo ossido con stato di ossidazione $+2$ a vanadio metallico tramite un'intermedia precipitazione del carburo di vanadio, come già evidenziato in precedenti studi. Questo comporta una maggiore complessità nella cinetica di riduzione degli ossidi di vanadio e precipitazione dei carburi, contestualmente al loro controllo per non peggiorare le proprietà finali del componente.